Simplified Equations for Shear Strength of Composite Concrete-Filled Steel Tubes

HADI KENARANGI, MICHEL BRUNEAU, AMIT H. VARMA, and
MUBASHSHIR AHMAD

ABSTRACT

Shear strength of filled composite members, namely, circular or rectangular concrete-filled steel tubes (CFST), have been investigated in past research. Results established the relative contributions of the steel tube and concrete infill to the total shear strength and showed that the concrete contribution depends on the development of a compression strut in the concrete infill when shear-span values are low. While experimental results and numerical models are available in the literature, simple equations that empirically encompass this behavior are preferable for design purposes. This paper provides an overview of the technical approach that has been followed to propose such equations for consideration and possible implementation in future editions of design specifications. The shear strength obtained using the proposed equation is compared with the shear test database from the existing literature and found to be safe; it accurately captures the contribution of the steel tube to the total shear strength and conservatively approximates that of the concrete.

Keywords: concrete-filled steel tubes, shear strength, composite behavior, mechanics-based equation, resistance factor, calibration, design.

INTRODUCTION AND BACKGROUND

Concrete-filled steel tubes (CFST) have a demonstrated ability to provide strength and ductility, which has made them desirable for both seismic and non-seismic applications (Bruneau and Marson, 2004; Hajjar, 2000; Hajjar et al., 2013; Han and Yang, 2005; Lai et al., 2017). Much research has demonstrated that these members can develop their plastic flexural strength (e.g., Bruneau and Marson, 2004; Lai et al., 2014; Leon et al., 2007; Roeder et al., 2010; Varma et al., 2002) and equations in design specifications typically account for full development of the plastic flexural strength of such members under combined bending and axial load.

Considerably less knowledge exists on the shear strength of such members. This may be attributable to challenges in experimentally developing the full shear strength of large concrete-filled tubes, and to the fact that shear is rarely a governing limit state for CFST members. For example, in the 2016 AISC *Specification for Structural Steel Buildings* (AISC, 2016b), hereafter referred to as the AISC *Specification*, the shear strength of composite concrete-filled tubes is specified to be either that of the steel section alone or that of the concrete section alone, presumably on the assumption that there exist few instances where a shear strength greater than this is necessary.

However, in some instances, more accurate prediction of this shear strength is desirable or needed. For example, this would be the case at the panel-zone locations of CFST columns in a composite moment frame (Fischer and Varma, 2014), or in CFST drilled shafts spanning across a thin, liquefiable soil layer located between two stiff layers during lateral spreading. In both of these cases, the CFST is subjected to double curvature bending over short lengths and subject to high resulting shear forces. In these cases, the shear strength of the CFST can become a significant consideration in its design.

It is important for design purposes to understand the physical behavior of composite CFST subjected to shear and to develop design equations that capture the respective contribution of the steel tube and concrete infill of the CFST to its total shear strength (contribution of internal reinforcement is not considered here for reasons described later). Design equations that are anchored in the mechanics of structural behavior provide more confidence in the design. For example, overestimating the strength of one component could result in an unexpected failure should that component become dominant in providing the total shear strength of that member.

Hadi Kenarangi, Structural and Earthquake Engineer, Modjeski and Masters, Inc., Mechanicsburg, Pa. Email: hkenarangi@modjeski.com (corresponding)

Michel Bruneau, SUNY Distinguished Professor, Department of Civil, Structural, and Environmental Engineering, University at Buffalo, Buffalo, N.Y. Email: bruneau@buffalo.edu

Amit H. Varma, Karl H. Kettelhut Professor, Lyles School of Civil Engineering, Purdue University, Ind. Email: ahvarma@purdue.edu

Mubashshir Ahmad, Graduate Student, Lyles School of Civil Engineering, Purdue University, Ind. Email: ahmad54@purdue.edu

Paper No. 2020-10

CIRCULAR CONCRETE-FILLED STEEL TUBES

The work presented in this section (1) summarizes recent research on the shear strength of circular concrete-filled members that illustrate the relative contributions of steel and concrete to the total shear strength and the contribution of a diagonal compression concrete strut to that strength (Kenarangi and Bruneau, 2020a, 2020b), (2) presents proposed (and calibrated) simplified design equations to simplify the more complex mechanics-based shear strength equation previously developed for composite CFST members (Kenarangi and Bruneau, 2020b), and (3) compares experimental results against the strength predicted by the proposed simplified equations.

2016 AISC *Specification* Shear Strength of Circular CFST

The shear strength of circular filled composite members given by the 2016 AISC *Specification* Section I4, is based on (1) the shear strength of the steel tube alone, (2) the available shear strength of the reinforced concrete portion alone, or (3) the shear strength of the steel tube plus the shear strength of the reinforcing steel.

Using this approach, for case 1, the shear strength of the circular steel tube alone using AISC *Specification* Equation G5-1 is:

$$V_{n(AISC)} = 0.5F_{cr}A_g \tag{1}$$

where $V_{n(AISC)}$ is the nominal shear strength of a circular steel tube and F_{cr} is the critical shear buckling stress taken as the larger of AISC *Specification* Equations G5-2a or G5-2b:

$$F_{cr} = \frac{1.6E_s}{\sqrt{\frac{L_v}{D}}\left(\frac{D}{t}\right)^{\frac{5}{4}}} \le 0.6F_y \tag{2}$$

$$F_{cr} = \frac{0.78E_s}{\left(\frac{D}{t}\right)^{\frac{3}{2}}} \le 0.6F_y \tag{3}$$

where

A_g = gross area of the steel tube cross section, in.^{2}
D = outside diameter of the steel tube, in.
E_s = modulus of elasticity of the steel, ksi
F_y = specified minimum yield stress of the steel tube, ksi
L_v = distance between points of maximum and zero shear, in.
t = design wall thickness, in.

Although not explicitly specified in AISC *Specification* Section I4, in concrete-filled steel tubes, the concrete fill provides support against buckling of the steel tube, and therefore, F_{cr} is taken as $0.6F_y$ for these sections. This would result in:

$$\begin{aligned} V_{n(AISC)} &= 0.5(0.6F_y)F_{cr}A_g \\ &= 0.3F_y\pi Dt \\ &= 0.94DtF_y \end{aligned}$$

Incidentally, this result corresponds to the first occurrence of yield at one point on the entire cross section (at its center in this case), as derived using classical equations to calculate elastic shear stresses (i.e., $\frac{V_yQ}{Ib}$, from any mechanics of materials textbook, with V_y calculated when the shear stress is τ_y).

For case 2, the shear strength of the concrete alone would be:

$$V_{c(ACI)} = 0.0632A_c\sqrt{f'_c} \tag{4}$$

where

A_c = area of the concrete section, in.^{2}
f'_c = uniaxial compressive strength of the concrete, ksi

Case 3 provides a marginal increase in shear strength over case 1, proportionally to how much the area of shear reinforcement adds to the area of the steel tube.

All the current AISC *Specification* Section I4 options are conservative and result in inefficient material use and increase in costs when shear governs the design.

Complex Shear Strength Equation

In order to investigate the behavior of circular CFST members under shear deformation, a series of finite element analyses were performed using element types and material models validated against experimental results, as described in more detail in Kenarangi and Bruneau (2020b). Analyses showed that a significant diagonal compression strut with a 45° angle developed in the concrete for some shear span-to-diameter (a/D) ratios. This is illustrated in Figure 1, which shows iso-surfaces for two different a/D ratios. To more clearly illustrate the development of the compression strut, principal stresses lower than 2.5 ksi are not shown in these figures. As a/D increases or decreases beyond the optimum case of $a/D = 0.5$ [which is the geometry shown in Figure 1(a)], the strength of the compression strut rapidly becomes less significant, as shown in Figure 1(b).

Based on observations from finite element analysis results, equations for the contribution of the infill concrete to the total shear strength of the CFST were developed. In these equations, the critical concrete strut cross section, A_{strut}, was located at the mid-length of the strut and was calculated from geometry to be:

$$A_{strut} = \frac{\sqrt{2}}{2}\left[4R_c^2 \arcsin\left(\frac{b}{2R_c}\right) + b\sqrt{4R_c{}^2 - b^2}\right] \quad (5)$$

where

$R_c = D_c/2$

$$b = \frac{D_c - H}{2} \qquad 0 \le b \le \frac{H}{2} \quad (6)$$

and

D_c = concrete core diameter, in.

H = height of the specimen in double curvature shear setup, which is equal to $2a$, in.

The resulting strut force, F_{strut}, calculated by multiplying A_{strut} by a uniformly distributed stress conservatively assumed to be equal to f_c', was then converted into horizontal (shear) and vertical (axial) force components, respectively, corresponding to the contribution to shear strength provided by the strut, V_{strut}, and a vertical force component of the strut, P_{strut}, transferred to the steel tube. Therefore,

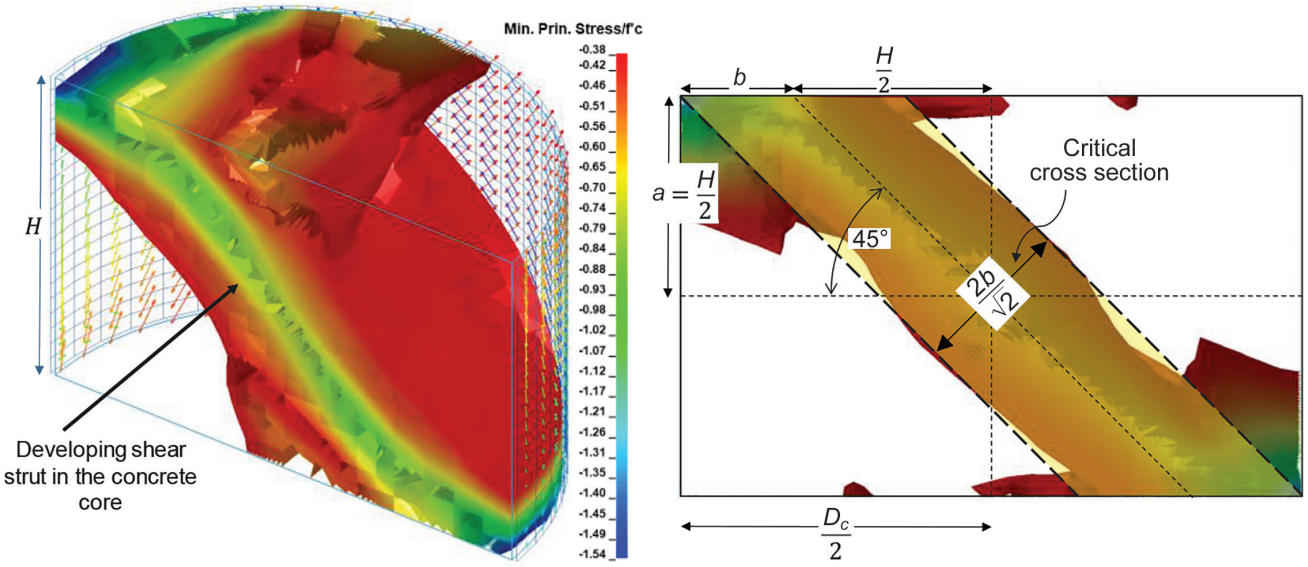

(a) $0.25 \le a/D \le 0.5$

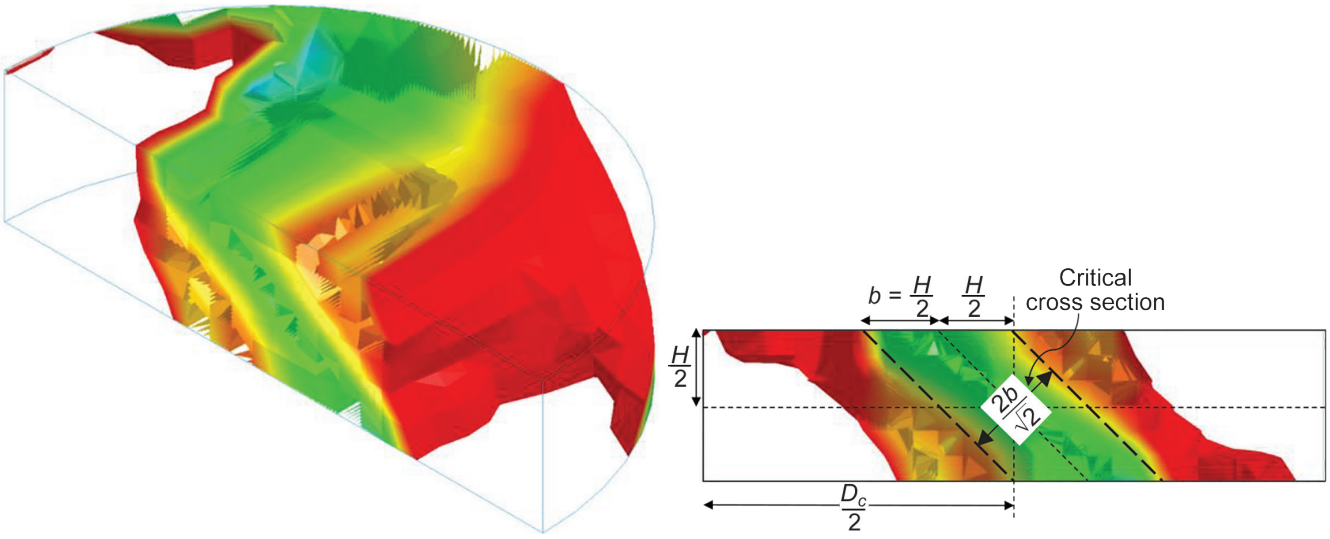

(b) $a/D < 0.25$

Fig. 1. Definition of diagonal compression strut in CFST.

$$V_{strut} = \frac{\sqrt{2}}{2} A_{strut} f_c' \tag{7a}$$

$$P_{strut} = \frac{\sqrt{2}}{2} A_{strut} f_c' \tag{7b}$$

At large shear span ratios, no strut develops, and the shear strength of the concrete defaults to the existing shear strength equations for concrete. Therefore, a lower limit of concrete shear strength, V_c, was defined here for V_{conc}, as shown in Equations 8 and 9. In Equation 9, the term outside the parenthesis is the nominal shear resistance of the concrete in accordance with ACI. The term inside the parenthesis was added to include the axial load effect on the shear resistance of the concrete. This term was adapted from ACI 318 (2011, 2014) Section 22.5.6 (which was the edition of ACI 318 in effect at the time this research was conducted).

$$V_{conc} = \max\left(V_{strut}, V_c\right) \tag{8}$$

where

$$V_c = 0.0632 A_c \sqrt{f_c'} \left(1 + \frac{P_{strut}}{2A_c}\right) \tag{9}$$

To calculate the nominal shear resistance of the steel tube, it was assumed that the tube cross section was fully yielded under combined tension and shear, and the effect of bending moment was neglected. In this case, the total shear resistance of the steel tube, V_s, can be calculated by integrating the maximum shear stress (which is tangent to the surface) over the steel tube cross section as shown in Figure 2 and calculated in Equation 10.

$$V_s = 2\int_{-\pi/2}^{\pi/2} \tau_{s,max} Rt \cos(\phi) d\phi \tag{10}$$

where R is the average radius of the steel tube and $\tau_{s,max}$ is the maximum shear stress on the steel tube cross section, calculated as:

$$\tau_{s,max} = \frac{1}{\sqrt{3}} \sqrt{F_y^2 - T^2} \tag{11}$$

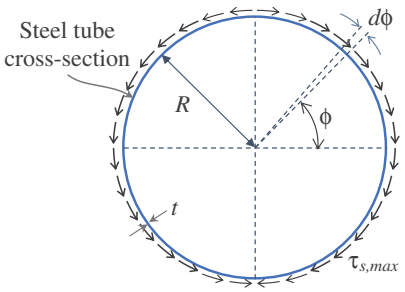

Fig. 2. Shear distribution on the steel tube cross section.

where F_y is the yield stress of the steel tube and $T = P_{strut}/A_s$ is the resultant tensile stress on the steel tube cross section due to the interaction of the concrete strut with the steel tube.

The resulting V_s obtained from Equation 10 is shown in Equation 12. The term under the square root shows that the shear strength of the steel tube reduces as the strut force increases, and P_{strut} should be less than $A_s F_y$. (Note: For a diagonal strut at 45°, $P_{strut} = V_{strut}$.)

$$V_s = \frac{2Dt}{\sqrt{3}} \sqrt{F_y^2 - \left(\frac{P_{strut}}{A_s}\right)^2} \tag{12}$$

Note that for all sections considered, the presence of P_{strut} was found to only have a marginal effect on the value of tube V_s. Also, in calculation of the shear contribution of the steel tube, the effect of the moment was neglected. This effect can be considered in the steel tube shear strength by including the stresses from bending moment using a similar but more complex equation (Kenarangi and Bruneau, 2020b).

Finally, the nominal shear strength of the composite CFST shaft was taken as equal to the summation of the shear strength of the concrete core and the steel tube, as shown in Equation 13.

$$V_{CFST} = V_s + V_{conc} \tag{13}$$

As mentioned before, the potential contribution of the reinforcing cage to the total shear strength is not included in this equation as it has a minimal contribution.

The proposed shear strength in Equation 13 was compared to finite element results with different shear span to diameter ratios. Figures 3(a) and 3(b) show the cases in which the bending moment is neglected or is included in calculation of the shear strength, respectively. In these figures the strengths were normalized to the summation of the strengths calculated by Equations 1 and 4. In these figures, M_p is the theoretical plastic flexural capacity of the section. The difference in the steel tube shear strength between these two cases is less than 8% for $a/D < 0.5$. This difference increases with the a/D ratio. Equations modified to account for the effect of axial load simultaneously acting on the cross section were also developed by Kenarangi and Bruneau (2020b), but these more complex equations are not presented here because the strength predicted by the equation used here was found to be adequately conservative in that case.

The proposed nominal shear strength obtained per these equations was compared with available test results by Kenarangi and Bruneau (2020a), Qian et al. (2007), Xu et al. (2009), Xiao et al. (2012), Nakahara and Tsumura (2014), Ye et al. (2016), and Roeder et al. (2016). Experimental

values were found to be, on average, 55% higher than the shear strength calculated by the proposed formula. To explain this result, Figure 4 shows cyclic hysteretic behavior obtained by finite element analysis for one of the specimens tested by Kenarangi and Bruneau (2020a) that failed under a shear dominant mode (note that none of the existing test data were tested under a pure shear condition because there is always a combination of flexure and shear at failure). In this figure, the shear forces carried by the steel tube and the infill concrete, as obtained from the finite element analysis, are compared with values at the maximum experimental strength point. This shows that at the displacement when the maximum experimentally obtained strength was reached, Equation 13 gives a good estimate of the shear strength resisted by the steel tube but underestimates the shear strength resisted by the concrete. This was done deliberately at the time as it was believed that this level of conservatism would be acceptable.

Simplified Shear Strength Equation for Circular CFST

Equations 5 through 13, while formulated to capture fundamental mechanisms that develop in CFST in shear, were deemed to be informative but too complex for practical use. Furthermore, while capturing well the contribution of steel to the total strength (and in a manner consistent with theoretical results from plastic analysis), they remained conservative when accounting for the contribution of the infill concrete to the total shear strength. The following alternative equation is therefore proposed, in a format that keeps the rational value derived for the contribution of steel to the total strength, and empirically increases the contribution of the concrete infill to match experimental results.

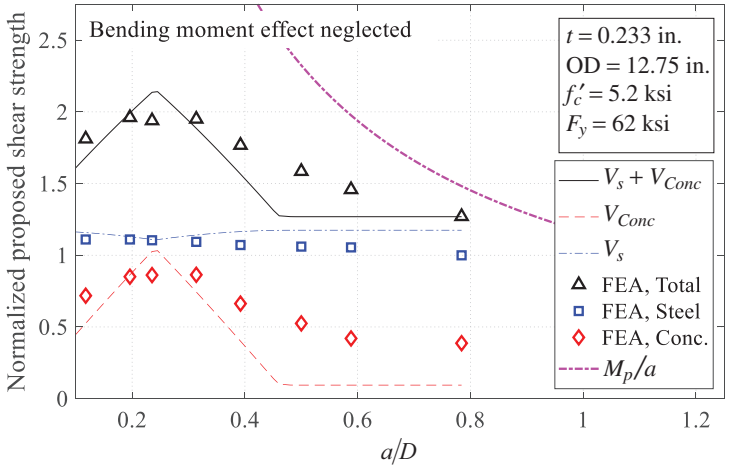

(a) Bending moment effects are neglected

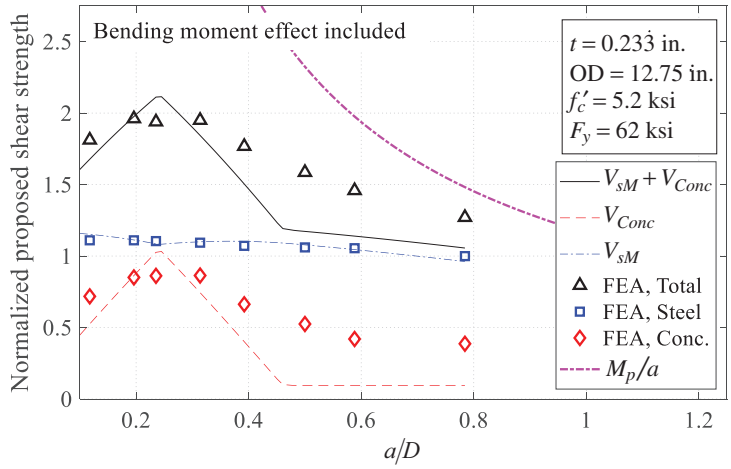

(b) Bending moment effects are included

Fig. 3. Normalized proposed shear strength vs. shear span to diameter ratios.

In this equation

$$V_n = V_s + V_c \tag{14}$$

where

$$V_s = \frac{2Dt}{\sqrt{3}} F_y = 1.15DtF_y \tag{15}$$

and

$$V_c = 0.0316\beta A_c \sqrt{f_c'} \tag{16}$$

in which the value of β is calibrated to be 18 and 20 for circular and rectangular CFST, respectively, for reasons explained in a subsequent section. Incidentally, this equation for V_s is the same one used in the Eurocode (CEN, 2005) as the upper strength limit for compact hollow circular tubes.

Note that while the proposed alternative shear strength equation does not explicitly consider the contribution of the developed compressive diagonal strut in the concrete, it empirically does so through the large β values used. Also note that the potential contribution of the reinforcing cage to the total shear strength is not included in the equations because the effect of the reinforcing cage was shown to have no significant impact on shear strength in experiments (Kenarangi and Bruneau, 2020a).

Experimental Database

For reasons mentioned earlier, there are a limited number of experimental tests developing the shear strength of circular CFST. The majority of these tests have been conducted using three- or four-point bending setups with simple end supports and under monotonic loadings (Roeder et al., 2016; Xiao et al., 2012; Xu et al., 2009). These test setups generate single curvature deflection along the member and, depending on the distance of the supports from each other, can produce flexure, flexure-shear, and shear dominant failures for long to short support distances, respectively. More representative of the loading likely to be experienced in panel zones, only some tests have considered specimens subjected to double-curvature deflection rather than single curvature, and even fewer have considered cyclic loading conditions. Monotonic double-curvature shear tests on small diameter CFST (4.7-in. diameter) have been performed by Ye et al. (2016) using a three-point bending setup and fixed support conditions at both ends. Cyclic double-curvature tests have been performed by Nakahara and Tsumura (2014) on 6.5-in.-diameter CFST and by Bruneau et al. (2018) on 12.75-in.- and 16-in.-diameter CFSTs with and without internal reinforcing cages, using a pantograph device to apply cyclic loading to specimens subjected to double-curvature deformations.

Summary of Experimental Results

The experimental tests considered here are listed in Table 1. In this table, D is the diameter of the steel tube; a is the clear span between the supports for single-curvature test setups and half of this value for the double-curvature test setups; P is the applied axial compressive load; and P_0 is the summation of yield strength of the steel tube and crushing capacity of the concrete, ignoring buckling (i.e., $P_0 = A_c f_c' + A_s F_y$). Note that only two sets of results were obtained

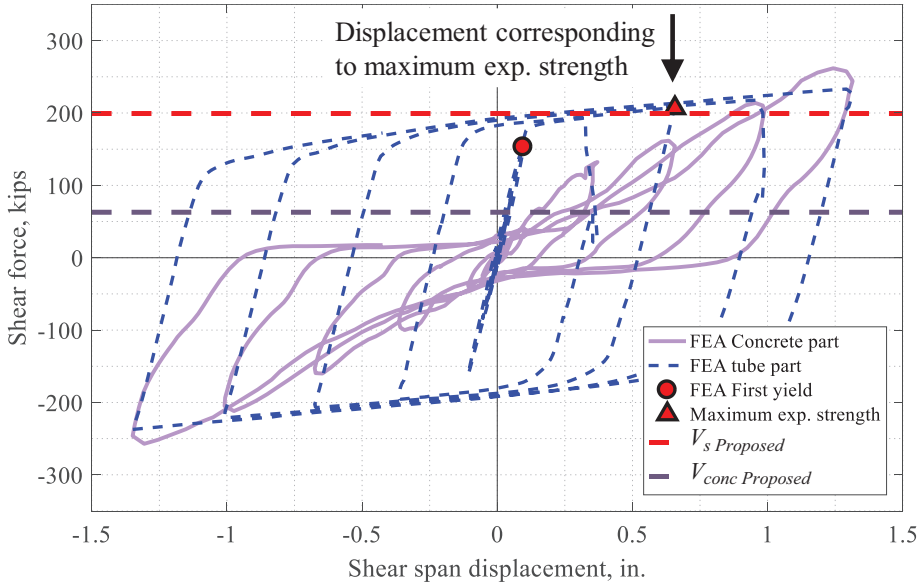

Fig. 4. Comparison of component shear forces of a 12.75-in.-diameter CFST tested by Kenarangi and Bruneau (2020a) with the proposed formula.

Table 1. Summary of the Existing Test Data on Shear Strength of Circular CFST Members					
Research	Test Setup	Loading Type	Diameter Range, in.	$\frac{a}{D}$ Range	$\frac{P}{P_0}$ Range
Bruneau et al. (2018)	Double curvature	Cyclic pantograph	12, 16	0.4	0
Roeder et al. (2016)	Single curvature	Monotonic four-point bending	20	0.25–1.0	0 and 0.085
Ye et al. (2016)	Double curvature	Monotonic three-point bending	4.7	0.15–0.75	0–0.73
Nakahara and Tsumura (2014)	Double curvature	Cyclic pantograph	6.5	0.5	0–0.4
Xiao et al. (2012)	Single curvature	Monotonic three-point bending	6.5	0.14–1.0	0–0.62
Xu et al. (2009)	Single curvature	Monotonic three-point bending	5.5	0.1–0.5	0

from cyclic loading, which was not deemed sufficient here to differentiate between results obtained from cyclic and monotonic loading.

Database for Shear Strength

For the Roeder et al. (2016) tests, the specimens that reportedly had a dominant flexural failure were excluded in the evaluation of the proposed shear formula. For the Ye et al. (2016) tests, the specimens with shear span-to-diameter ratio of less than 0.1 were also excluded. The Qian et al. (2007) tests on specimens with a low-shear span-to-diameter ratio (typically 0.1) were not considered here due to suspiciously high strength compared to all other researchers' results (with $V_{exp}/V_{simplified}$ values as high as 3.48). For all the existing test results, any test with $M_{exp}/M_p > 1.15$ was considered as a flexural dominant failure and was excluded from evaluations. The plastic moment, M_p, is the composite section plastic moment calculated using the plastic stress distribution method (PSDM). A few cases for which $1.0 < M_{exp}/M_p < 1.15$ were included when they were reported by the original researchers as failing in shear.

Also, it should be noted that not all the tested specimens may have exhibited a shear failure mode. The test result observations provided by Xiao et al. (2012) and Ye et al. (2016) for specimens having a/D values as low as 0.1 and 0.15 suggest that some of those specimens may have had a mixed failure mode of shear combined with other local-crushing phenomena.

Comparison of Experimental Results with Shear Strength Equations

To compare with experimental results, the ratios of the shear strength obtained experimentally and obtained using the proposed equation have been calculated for the available test data (Bruneau et al., 2018; Nakahara and Tsumura, 2014; Roeder et al., 2016; Xiao et al., 2012; Xu et al., 2009; Ye et al., 2016). Results are presented in Tables 2 and 3 for tests with and without axial load, respectively.

Values of the ratio of the strengths of the existing shear tests, V_{exp}, to their corresponding shear strengths calculated by the proposed simplified equation, V_{CFST}, are plotted in Figure 5 for specimens for which no axial load was applied. Note that values of the experimentally applied moments to the plastic moment, M_{exp}/M_p, included in Tables 2 and 3 show that the values plotted here correspond to specimens that exhibited shear-dominant failures (i.e., not flexure-dominant failures). Maximum calculated ratio of M_{exp}/M_p for the tests plotted in Figure 5 is 1.05. The horizontal axis in this figure represents the shear span-to-diameter ratio, a/D. The mean and standard deviation values of the results are included in the figure. As shown, on average, the experimental values are about 11% more than the values predicted by the proposed simplified formula.

The experimental-to-proposed simplified shear strength ratios for all the available test data, also including specimens for which axial load was applied, are shown in Figure 6. Figure 6(a) shows the ratio of experimental to calculated shear strengths versus the applied external axial load, and Figure 6(b) shows this ratio versus the shear span-to-diameter ratio. As shown, on average, the experimental values are about 35% more than the values predicted by the proposed formula. According to Figure 6(a), the proposed formula gives particularly more conservative values for the cases with more than $0.5P/P_0$ applied axial load. Also, Figure 6(b) shows that the predicted values using the proposed formula is more conservative for a/D ratios of less than 0.2. Maximum calculated ratio of M_{exp}/M_p for all the considered specimens, including the axial load, is 1.12.

While the results obtained with the proposed simplified

Table 2. Existing Experiments—Properties, Results, and Comparison with the Proposed Equation for Tests without Axial Load																
Specimen	D (in.)	a (in.)	$\frac{a}{D}$	t (in.)	$\frac{D}{t}$	f'_c (ksi)	E_c (ksi)	F_y (ksi)	$\frac{P}{P_0}$	P (kips)	V_{exp} (kips)	V_{CFST} (kips)	$\frac{V_{exp}}{V_{CFST}}$	M_{exp} (kip-in.)	M_p (kip-in.)	$\frac{M_{exp}}{M_p}$
Bruneau et al. (2018)																
KB1	16.0	6.5	0.41	0.232	68.8	2.9	2757	51	0	0	437	401	1.09	2841	3428	0.83
KB3	12.8	5.0	0.39	0.232	54.8	4.5	3434	58	0	0	396	342	1.16	1980	2489	0.80
KB4	12.8	5.0	0.39	0.232	54.8	4.5	3434	58	0	0	397	342	1.16	1985	2489	0.80
KB5	12.8	5.0	0.39	0.232	54.8	4.5	3434	58	0	0	414	342	1.21	2070	2489	0.83
KB6	12.8	5.0	0.39	0.232	54.8	4.5	3434	58	0	0	407	342	1.19	2035	2489	0.82
KB7	12.8	5.0	0.39	0.232	54.8	4.5	3434	58	0	0	404	342	1.18	2020	2489	0.81
Roeder et al. (2016)																
R12	20	10	0.5	0.233	86	6.2	4031	54	0	0	651	714	0.91	6510	6211	1.05
R19	20	10	0.5	0.349	57	9.1	4891	57	0	0	952	964	0.99	9520	9684	0.98
R7	20	7.5	0.38	0.233	86	6.5	4111	50	0	0	705	702	1.00	5288	5826	0.91
R8	20	7.5	0.38	0.233	86	6.5	4121	54	0	0	802	723	1.11	6015	6233	0.96
R10	20	7.5	0.38	0.233	86	6.2	4014	54	0	0	665	712	0.93	4988	6207	0.80
R11	20	7.5	0.38	0.233	86	6.6	4162	57	0	0	600	743	0.81	4500	6551	0.69
R16	20	7.5	0.38	0.233	86	8.6	4750	57	0	0	765	805	0.95	5738	6691	0.86
R21	20	7.5	0.38	0.233	86	0.0	0	57	0	0	449	305	1.47	3368	5160	0.65
R14	20	5.0	0.25	0.233	86	8.6	4747	55	0	0	826	797	1.04	4130	6538	0.63
R15	20	5.0	0.25	0.233	86	8.8	4802	55	0	0	796	803	0.99	3980	6550	0.61
R20	20	5.0	0.25	0.233	86	2.8	2704	57	0	0	712	590	1.21	3560	6089	0.58
Ye et al. (2016)																
Ye1	4.7	0.7	0.15	0.079	60	4.6	3481	49	0	0	54	41	1.31	38	101	0.38
Ye2	4.7	0.7	0.15	0.079	60	4.6	3481	49	0	0	54	41	1.32	39	101	0.38
Nakahara and Tsumura (2014)																
N1	6.5	3.3	0.5	0.193	33.9	9.3	5336	79	0	0	150	166	0.90	491	713	0.69
Xiao et al. (2012)																
X1	6.3	2.5	0.40	0.217	29	3.8	3137	55	0	0	141	116	1.21	354	485	0.73
X2	6.3	2.5	0.40	0.217	29	4.7	3509	55	0	0	152	119	1.27	382	492	0.78
X3	6.3	2.5	0.40	0.217	29	4.3	3348	55	0	0	146	118	1.24	368	489	0.75
X4	6.5	2.6	0.40	0.173	38	3.8	3137	50	0	0	116	99	1.17	301	399	0.75
X5	6.5	2.6	0.40	0.173	38	4.7	3509	50	0	0	128	102	1.24	332	406	0.82
X6	6.5	2.6	0.40	0.173	38	4.3	3348	50	0	0	118	101	1.17	307	403	0.76
X7	6.5	2.6	0.40	0.118	55	3.8	3137	59	0	0	84	86	0.98	219	329	0.66
X8	6.5	2.6	0.40	0.118	55	4.7	3509	59	0	0	93	90	1.03	242	336	0.72
X9	6.5	2.6	0.40	0.118	55	4.3	3348	59	0	0	87	89	0.98	225	333	0.68
X25	6.3	0.9	0.14	0.217	29	3.8	3137	55	0	0	112	116	0.97	97	485	0.20
X26	6.3	0.9	0.14	0.217	29	4.7	3509	55	0	0	118	119	0.99	102	492	0.21
X27	6.3	0.9	0.14	0.217	29	4.3	3348	55	0	0	124	118	1.05	107	489	0.22
X28	6.3	0.9	0.14	0.217	29	4.3	3348	55	0	0	157	118	1.33	136	489	0.28
X29	6.5	0.9	0.14	0.173	38	4.3	3348	50	0	0	146	101	1.45	132	403	0.33
X30	6.5	0.9	0.14	0.118	55	4.3	3348	59	0	0	101	89	1.14	92	333	0.28
X31	6.5	0.9	0.14	0.173	38	3.8	3137	50	0	0	118	99	1.20	107	399	0.27
X32	6.5	0.9	0.14	0.173	38	4.7	3509	50	0	0	129	102	1.26	117	406	0.29
X33	6.5	0.9	0.14	0.173	38	4.3	3348	50	0	0	126	101	1.25	115	403	0.28
X34	6.5	0.9	0.14	0.118	55	3.8	3137	59	0	0	90	86	1.04	81	329	0.25

Table continues on the next page

Table 2. Existing Experiments—Properties, Results, and Comparison with the Proposed Equation for Tests without Axial Load (continued)																
Specimen	D (in.)	a (in.)	$\frac{a}{D}$	t (in.)	$\frac{D}{t}$	f'_c (ksi)	E_c (ksi)	F_y (ksi)	$\frac{P}{P_0}$	P (kips)	V_{exp} (kips)	V_{CFST} (kips)	$\frac{V_{exp}}{V_{CFST}}$	M_{exp} (kip-in.)	M_p (kip-in.)	$\frac{M_{exp}}{M_p}$
Xiao et al. (2012) (continued)																
X35	6.5	0.9	0.14	0.118	55	4.7	3509	59	0	0	96	90	1.06	87	336	0.26
X36	6.5	0.9	0.14	0.118	55	4.3	3348	59	0	0	92	89	1.04	83	333	0.25
X55	6.3	3.2	0.50	0.256	25	2.9	2764	65	0	0	169	147	1.15	538	652	0.82
X57	6.5	3.3	0.50	0.161	40	2.9	2764	59	0	0	99	101	0.99	324	425	0.76
Xu et al. (2009)																
Xu16	5.5	0.6	0.1	0.145	38	4.9	3576	53	0	0	93	76	1.23	51	255	0.20
Xu17	5.5	1.1	0.2	0.145	38	4.9	3576	53	0	0	83	76	1.10	91	255	0.36
Xu18	5.5	1.7	0.3	0.145	38	4.9	3576	53	0	0	80	76	1.06	132	255	0.52
Xu19	5.5	2.8	0.5	0.145	38	4.9	3576	53	0	0	68	76	0.90	188	255	0.74
Xu26	5.5	0.6	0.1	0.145	38	4.9	3576	53	0	0	88	76	1.16	188	255	0.74
Xu27	5.5	1.1	0.2	0.145	38	4.9	3576	53	0	0	79	76	1.04	48	255	0.19
Xu28	5.5	1.7	0.3	0.145	38	4.9	3576	53	0	0	75	76	0.99	87	255	0.34

Table 3. Existing Experiments—Properties, Results, and Comparison with the Proposed Equation for Tests with Axial Load																
Specimen	D (in.)	a (in.)	$\frac{a}{D}$	t (in.)	$\frac{D}{t}$	f'_c (ksi)	E_c (ksi)	F_y (ksi)	$\frac{P}{P_0}$	P (kips)	V_{exp} (kips)	V_{CFST} (kips)	$\frac{V_{exp}}{V_{CFST}}$	M_{exp} (kip-in.)	M_p (kip-in.)	$\frac{M_{exp}}{M_p}$
Roeder et al. (2016)																
R13	20	7.5	0.38	0.233	86	5.3	3737	54	0.09	202	710	683	1.04	5325	6134	0.87
Ye et al. (2016)																
Ye3	4.7	0.7	0.15	0.079	60	4.6	3481	49	0.24	32	60	41	1.47	43	101	0.42
Ye4	4.7	0.7	0.15	0.079	60	4.6	3481	49	0.24	32	57	41	1.38	40	101	0.40
Ye5	4.7	0.7	0.15	0.079	60	4.6	3481	49	0.59	78	71	41	1.73	51	101	0.50
Ye6	4.7	0.7	0.15	0.079	60	4.6	3481	49	0.59	78	72	41	1.74	51	101	0.50
Ye7	4.7	0.7	0.15	0.079	60	4.6	3481	49	0.73	97	75	41	1.82	53	101	0.53
Ye8	4.7	0.7	0.15	0.079	60	4.6	3481	49	0.73	97	71	41	1.73	51	101	0.50
Ye11	4.7	0.7	0.15	0.079	60	4.6	3481	49	0.49	65	65	41	1.58	46	101	0.46
Ye12	4.7	0.7	0.15	0.079	60	4.6	3481	49	0.49	65	64	41	1.56	45	101	0.45
Ye13	4.7	2.4	0.5	0.079	60	4.6	3481	49	0.49	65	39	41	0.96	93	101	0.92
Ye14	4.7	2.4	0.5	0.079	60	4.6	3481	49	0.49	65	44	41	1.06	103	101	1.02
Ye17	4.7	0.7	0.15	0.079	60	8.3	4670	49	0.34	65	79	48	1.65	56	106	0.53
Ye18	4.7	0.7	0.15	0.079	60	8.3	4670	49	0.34	65	76	48	1.58	54	106	0.51
Ye19	4.7	0.7	0.15	0.118	40	4.6	3481	60	0.37	65	88	58	1.51	62	173	0.36
Ye20	4.7	0.7	0.15	0.118	40	4.6	3481	60	0.37	65	88	58	1.51	62	173	0.36
Nakahara and Tsumura (2014)																
N2	6.3	3.1	0.5	0.089	70	9.6	5655	73	0.1	41	109	99	1.10	343	316	1.08
N3	6.5	3.3	0.5	0.193	33	9.3	5336	79	0.3	174	162	166	0.98	530	713	0.74
N4	6.3	3.1	0.5	0.089	70	9.6	5655	73	0.3	123	96	99	0.97	303	316	0.96
N5	6.5	3.3	0.5	0.197	33	7.0	4887	79	0.1	51	153	160	0.96	501	700	0.72
N6	6.5	3.3	0.5	0.197	33	7.0	4887	79	0.2	102	156	160	0.98	508	700	0.73
N7	6.5	3.3	0.5	0.197	33	7.0	4887	79	0.4	205	148	160	0.93	484	700	0.69
N8	6.3	3.1	0.5	0.089	70	9.6	5655	73	0.15	61	102	99	1.03	321	316	1.02
N9	6.3	3.1	0.5	0.089	70	9.6	5655	73	0.2	82	112	99	1.13	354	316	1.12

Table continues on the next page

Table 3. Existing Experiments—Properties, Results, and Comparison with the Proposed Equation for Tests with Axial Load (continued)																
Specimen	D (in.)	a (in.)	$\frac{a}{D}$	t (in.)	$\frac{D}{t}$	f'_c (ksi)	E_c (ksi)	F_y (ksi)	$\frac{P}{P_0}$	P (kips)	V_{exp} (kips)	V_{CFST} (kips)	$\frac{V_{exp}}{V_{CFST}}$	M_{exp} (kip-in.)	M_p (kip-in.)	$\frac{M_{exp}}{M_p}$
Xiao et al. (2012)																
X10	6.3	2.5	0.40	0.217	29	3.8	3137	55	0.32	105	164	116	1.41	412	485	0.85
X11	6.3	2.5	0.40	0.217	29	4.7	3509	55	0.31	109	169	119	1.41	425	492	0.86
X12	6.3	2.5	0.40	0.217	29	4.3	3348	55	0.31	106	175	118	1.49	442	489	0.90
X13	6.5	2.6	0.40	0.173	38	3.8	3137	50	0.31	89	142	99	1.44	368	399	0.92
X14	6.5	2.6	0.40	0.173	38	4.7	3509	50	0.30	94	147	102	1.43	381	406	0.94
X15	6.5	2.6	0.40	0.173	38	4.3	3348	50	0.30	90	152	101	1.51	394	403	0.98
X16	6.5	2.6	0.40	0.118	55	3.8	3137	59	0.30	77	108	86	1.25	280	329	0.85
X17	6.5	2.6	0.40	0.118	55	4.7	3509	59	0.28	80	109	90	1.21	283	336	0.84
X18	6.5	2.6	0.40	0.118	55	4.3	3348	59	0.28	77	111	89	1.26	289	333	0.87
X19	6.3	2.5	0.40	0.217	29	3.8	3137	55	0.64	210	158	116	1.36	398	485	0.82
X20	6.3	2.5	0.40	0.217	29	4.7	3509	55	0.62	219	182	119	1.52	459	492	0.93
X21	6.5	2.6	0.40	0.173	38	3.8	3137	50	0.62	179	146	99	1.48	380	399	0.95
X22	6.5	2.6	0.40	0.173	38	4.7	3509	50	0.60	188	157	102	1.54	409	406	1.01
X23	6.5	2.6	0.40	0.118	55	3.8	3137	59	0.60	154	123	86	1.42	318	329	0.97
X24	6.5	2.6	0.40	0.118	55	4.7	3509	59	0.56	160	130	90	1.44	339	336	1.01
X37	6.3	0.9	0.14	0.217	29	3.8	3137	55	0.32	105	202	116	1.75	175	485	0.36
X38	6.3	0.9	0.14	0.217	29	4.7	3509	55	0.31	109	225	119	1.88	195	492	0.40
X39	6.3	0.9	0.14	0.217	29	4.3	3348	55	0.31	106	214	118	1.81	185	489	0.38
X40	6.5	0.9	0.14	0.173	38	3.8	3137	50	0.31	89	185	99	1.88	168	399	0.42
X41	6.5	0.9	0.14	0.173	38	4.7	3509	50	0.30	94	202	102	1.97	183	406	0.45
X42	6.5	0.9	0.14	0.173	38	4.3	3348	50	0.30	90	191	101	1.90	173	403	0.43
X43	6.5	0.9	0.14	0.118	55	3.8	3137	59	0.30	77	152	86	1.76	137	329	0.42
X44	6.5	0.9	0.14	0.118	55	4.7	3509	59	0.28	80	169	90	1.87	153	336	0.45
X45	6.5	0.9	0.14	0.118	55	4.3	3348	59	0.28	77	157	89	1.78	143	333	0.43
X46	6.3	0.9	0.14	0.217	29	3.8	3137	55	0.64	210	211	116	1.82	183	485	0.38
X47	6.3	0.9	0.14	0.217	29	4.7	3509	55	0.62	219	236	119	1.98	204	492	0.42
X48	6.3	0.9	0.14	0.217	29	4.3	3348	55	0.62	211	270	118	2.29	234	489	0.48
X49	6.5	0.9	0.14	0.173	38	3.8	3137	50	0.62	179	230	99	2.34	209	399	0.52
X50	6.5	0.9	0.14	0.173	38	4.7	3509	50	0.60	188	236	102	2.30	214	406	0.53
X51	6.5	0.9	0.14	0.173	38	4.3	3348	50	0.60	180	202	101	2.01	183	403	0.45
X52	6.5	0.9	0.14	0.118	55	3.8	3137	59	0.60	154	172	86	1.99	156	329	0.47
X53	6.5	0.9	0.14	0.118	55	4.7	3509	59	0.56	160	185	90	2.05	168	336	0.50
X54	6.5	0.9	0.14	0.118	55	4.3	3348	59	0.57	155	193	89	2.18	175	333	0.53

equation are safe even when including the results from Xiao et al. (2012) and Ye et al. (2016) with a/D ratios less than or equal to 0.15 (as shown in Figure 6), by excluding the test results of $a/D \leq 0.15$, the mean value of experimental-to-proposed shear strengths would improve to 1.15 with a lower standard deviation of 0.19.

The shear strengths from the steel tube and concrete infill of a circular CFST calculated by the proposed simplified equation for different shear span ratios are shown in Figure 7. Results from monotonic finite element analyses are also shown in this figure for comparison. This figure shows how the simplified equation compares to the finite element analyses results for different shear span to depth ratios.

RECTANGULAR CONCRETE-FILLED STEEL TUBES

This section presents for rolled and built-up rectangular (and square) CFST: the experimental database, proposed simplified shear strength equation, and comparison of calculated to experimental shear strengths.

Experimental Database

Compared to circular CFST, fewer shear tests on rectangular CFST are found in the literature. The shear tests available in the literature can be categorized based on the type of loading and test setup used. For example, tests have been conducted using (1) a pantograph type test setup, (2) a three- or four-point beam bending type test setup, and (3) a beam-to-column subassembly type test setup for panel-zone shear. The experimental database, described in the following subsections, includes tests with shear span-to-depth (a/D) ratios ranging from 0.075 to 1.5; axial load ratios (P/P_0) ratios ranging from 0.0 to 0.65; plate slenderness ratios (D/t) ranging from 21 to 67; concrete compressive strength, f_c', ranging from 2.4 to 17 ksi; and steel yield stress, F_y, ranging from 42 to 117 ksi. In the following discussion and database, a is the shear span defined by the loading during the test; D is the total depth of the specimen in the direction of shear loading; P is the applied compressive axial force; P_0 is the section axial capacity of the rectangular CFST calculated as the sum of the steel yield strength, A_sF_y, and the concrete compressive strength, A_cf_c'; b is the width of the CFST member; t is the thickness of the steel tube; f_c' is the uniaxial compressive strength of concrete; F_y is the yield strength of steel; A_s is the cross-sectional area of steel tube; and A_c is the cross-sectional area of the concrete infill. Tests with an a/D ratio greater than 1.5 exhibit flexure-dominant behavior and, therefore, have been excluded in this study.

Tomii and Sakino (1979) were one of the earliest researchers to investigate the fundamental flexure and shear behavior of rectangular CFST members. Forty small-scale specimens were tested and categorized into five series of tests, depending on the parameter values. Sakino and Ishibashi (1985) continued the work and conducted tests on 21 small-scale specimens that could be categorized into six series based on the parameters. Both research studies were conducted using the same pantograph type test setup that subjected the specimens to double-curvature bending under constant axial load and monotonic or cyclic shearing force.

Koester (2000) conducted experimental investigations to evaluate the fundamental shear behavior of rectangular CFST members and the panel-zone behavior of rectangular CFST-to-steel beam connections. The connection panel-zone region was idealized as shown in Figure 8, and a schematic view of the test setup is shown in Figure 9. This paper only includes the specimens exhibiting shear failure and having regular steel tube geometry (no cutouts, etc.).

Koester (2000) also conducted six full-scale tests on subassemblies consisting of square CFST column-to-steel beam moment connections, where the moment connections were split-tee. through-bolted moment connections. The tests were conducted by subjecting the subassembly specimens to cyclic lateral loading using the schematic shown in Figure 10. Ricles et al. (2004) supplemented the research

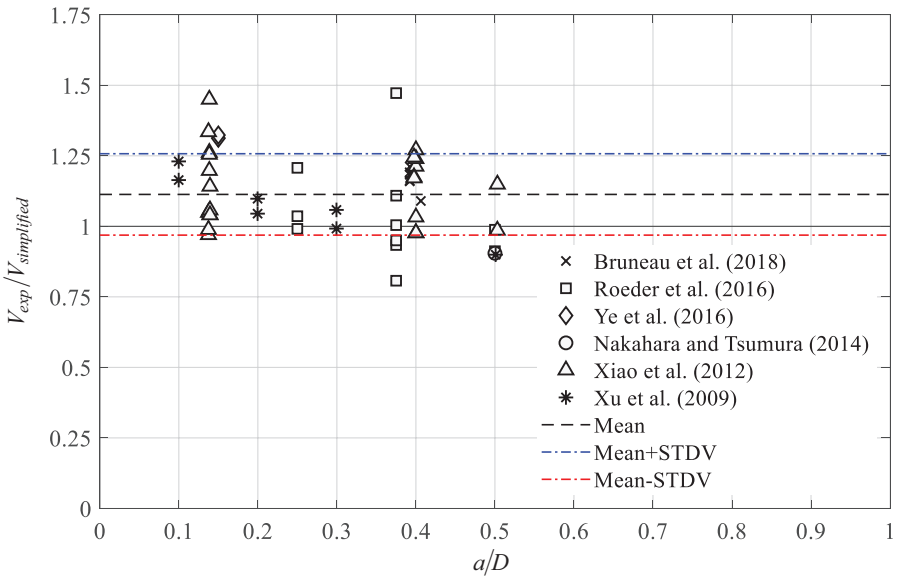

Fig. 5. Ratio of strength from existing test results with no axial load to proposed simplified shear strength formula as a function of shear span, a/D.

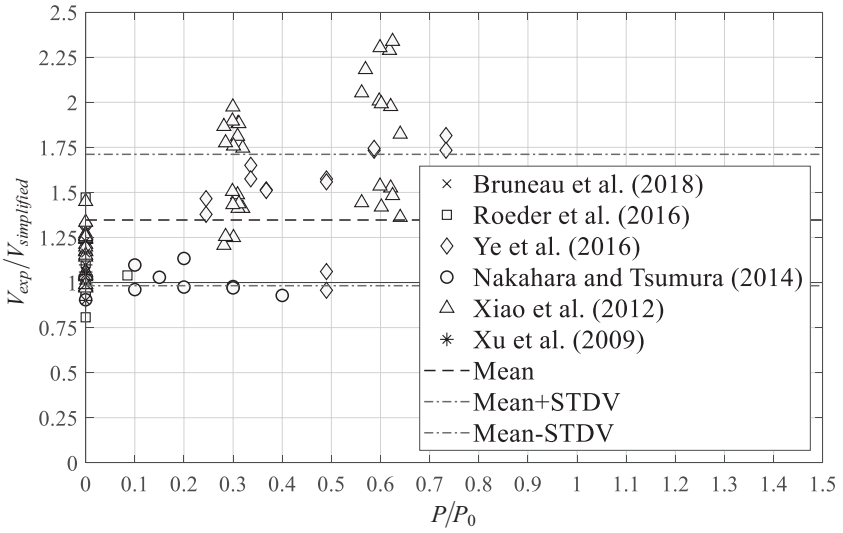

(a) Normalized applied axial load, P/P$_0$

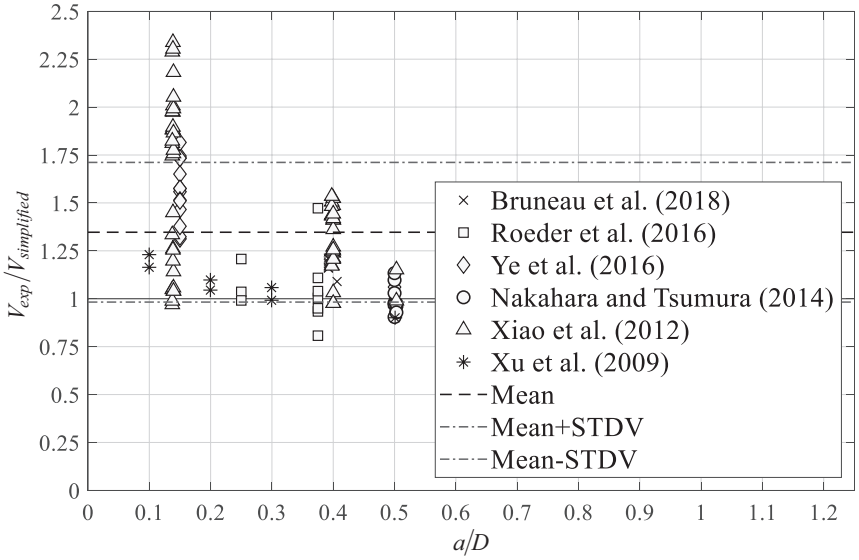

(b) Shear span, a/D

Fig. 6. Ratio of strength from existing test results to proposed simplified shear strength formula.

conducted by Koester (2000) and evaluated the seismic behavior of two interior joint type subassemblies consisting of square CFST columns—steel beam moment connections with weak panel zones. The panel zones had interior steel plate diaphragms that were complete joint penetration welded on only three or four sides.

Nishiyama et al. (2004) studied the effect of high-strength concrete and steel material on the shear strength of the panel zone of CFST column-to-steel beam joint subassemblies. Five specimens consisting of subassemblies made from square CFST columns and steel beams were tested. Both interior and exterior joint types with through and outer diaphragms were studied. The specimens were designed to fail under panel-zone shear by reducing the thickness of the CSFT steel tube in the panel zone. The axial load on columns was held constant as a reversed cyclic lateral load was applied at the beam ends, as shown in Figure 11. Fukumoto and Morita (2005) continued the work and presented three more tests on interior joint type steel beam-square CFST column subassemblies with interior diaphragms.

Wu et al. (2005) studied the seismic behavior of square CFST column-to-steel beam joints by testing three interior joint type subassemblies using a setup similar to Figure 11. Shawkat et al. (2008) tested four rectangular CFST under three-point bending in a displacement-controlled mode. Ye et al. (2016) tested 18 small-scale specimens under various combinations of axial compression and shear. The specimens were fixed at the ends, subjected to constant axial

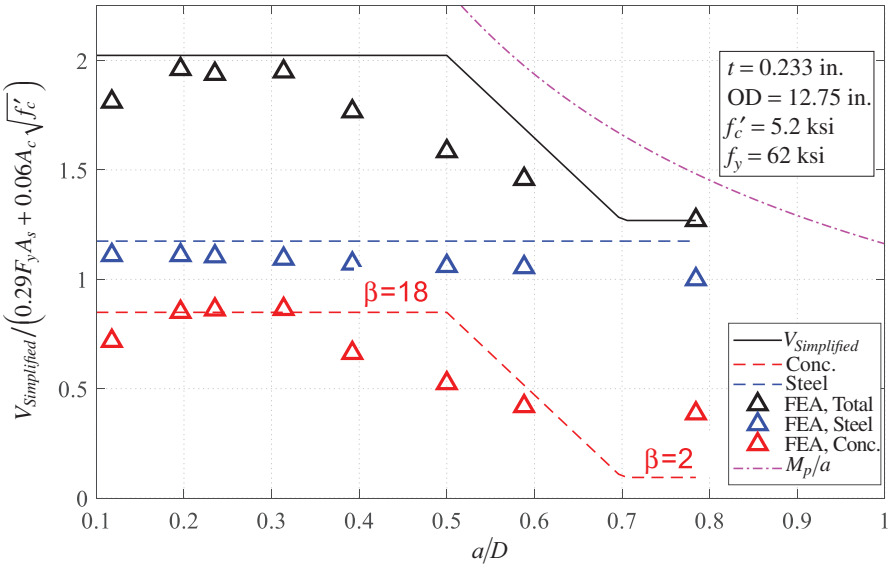

Fig. 7. Normalized proposed simplified shear strength vs. shear span-to-diameter ratios.

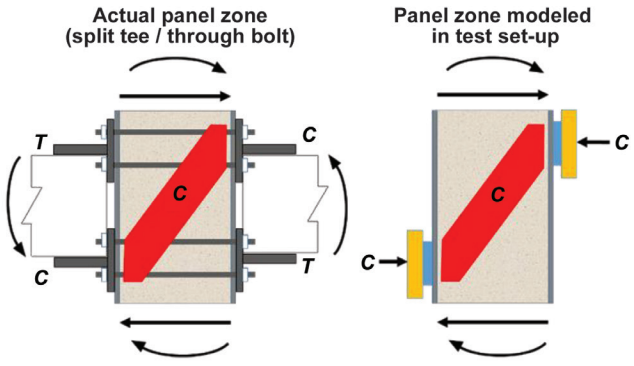

Fig. 8. Panel-zone region in connections and idealization for testing (adapted from Koester, 2000).

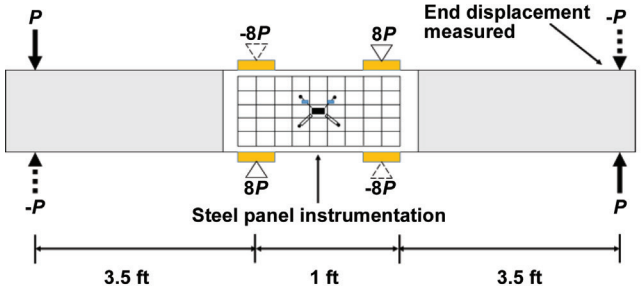

Fig. 9. Schematic view of test setup for idealized small-scale specimens (adapted from Koester, 2000).

loading, and tested under monotonic three-point bending to produce double curvature using the test setup with schematic shown in Figure 12.

Summary of Results

The compiled experimental database is summarized in Table 4 along with the relevant parameters, including test setup; loading type; cross-section dimensions; shear span-to-depth ratio, a/D; and axial load ratio, P/P_0. The general conclusions and results from the research database are as follows:

1. Rectangular CFST are typically flexure critical and very difficult to fail in shear due to their high shear strength, which includes contributions from the webs of the steel tube and the concrete infill (Tomii and Sakino, 1979; Koester, 2000).
2. Changing the failure mode from flexure critical to shear critical depends primarily on the shear span-to-depth ratio, a/D. The a/D ratio has to be made extremely small (<1.0) to force shear failure. Specimens with $1.0 \leq a/D < 3.0$ generally fail in combined shear and flexure, and specimens with $a/D \geq 3.0$ generally fail in flexure (Sakino and Ishibashi, 1985).

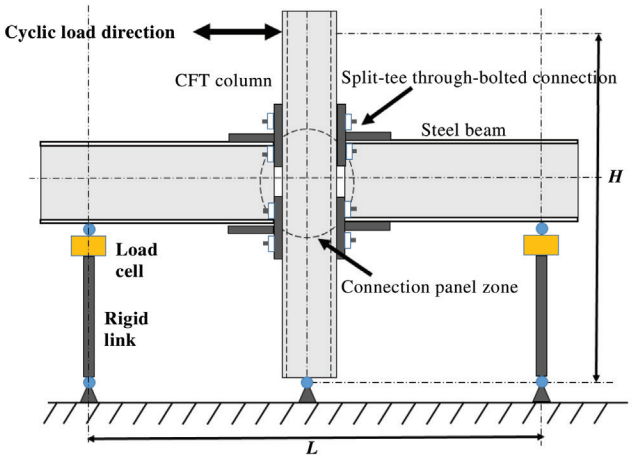

Fig. 10. Schematic view of test setup with cyclic lateral loading applied at column top (adapted from Koester, 2000).

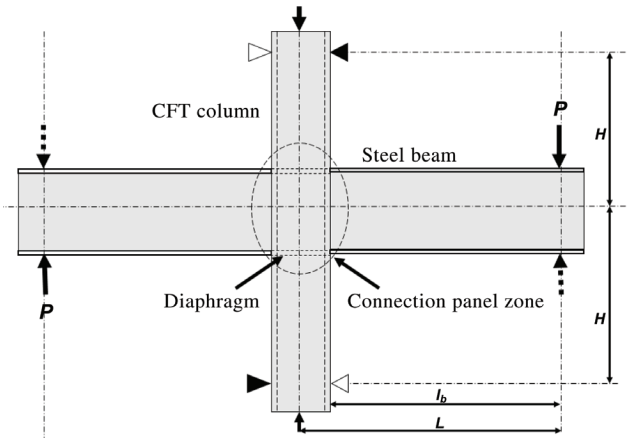

Fig. 11. Schematic view of test setup with cyclic loading applied at beam ends (adapted from Nishiyama et al., 2004).

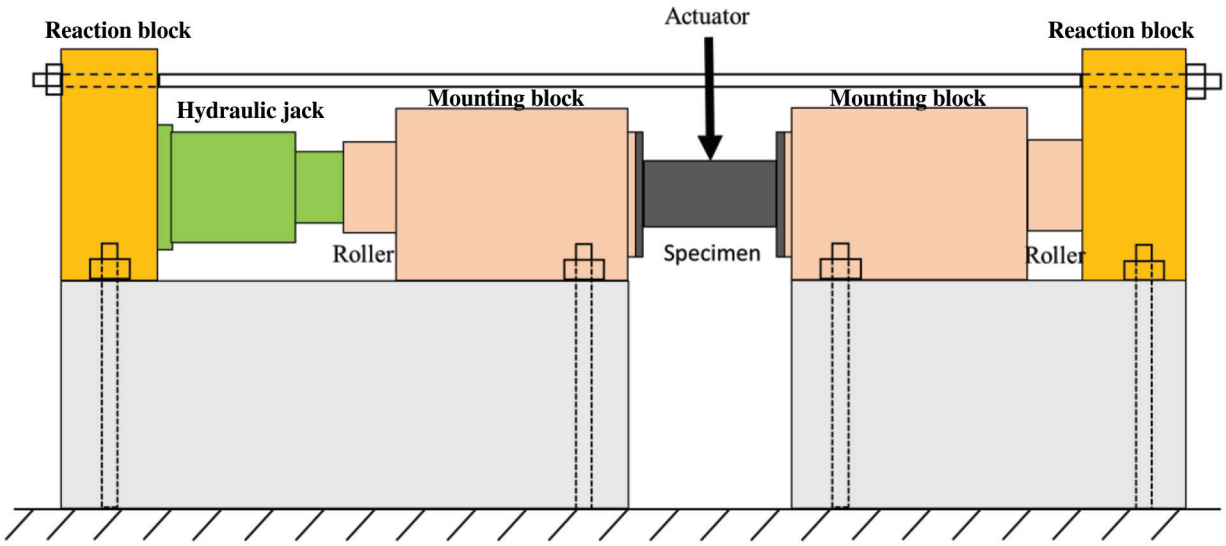

Fig. 12. Schematic view of the test setup (adapted from Ye et al., 2016).

Table 4. Summary of the Existing Test Data on Shear Strength of RCFST Members					
Research	**Test Setup**	**Loading Type**	**Section, in. × in.**	**a/D Range**	**P/P_0 Range**
Tomii and Sakino (1979)	Pantograph	Double-curvature bending	3.9 × 3.9	0.83–1	0–0.5
Sakino and Ishibashi (1985)	Pantograph	Double-curvature bending	3.9 × 3.9	1–1.5	0–0.5
Koester (2000)	Four-point bending	Cyclic bending	8 × 8, 12 × 12, 16 × 16	0.75	0
Ricles et al. (2004)	Beam-to-column Subassembly	Cyclic lateral loading	16 × 16	0.75	0.12
Nishiyama et al. (2004)	Beam-to-column Subassembly	Cyclic lateral loading	9.8 × 9.8, 6.4 × 6.4	0.5	0.2–0.65
Fukumoto and Morita (2005)	Beam-to-column Subassembly	Monotonic lateral loading	7.9 × 7.9	0.75	0
Wu et al. (2005)	Beam-to-column Subassembly	Cyclic lateral loading	15.7 × 15.7	0.6	0.16–0.19
Shawkat et al. (2008)	Three-point bending	Monotonic bending	4.0 × 5.9	1.0	0
Ye et al. (2016)	Three-point bending	Monotonic bending	4.7 × 4.7	0.075–0.75	0–0.65

3. Applying axial compression (P/P_0) further increases the shear strength of specimens (Ye et al., 2016). This increase is due to the reduction in concrete cracking and increase in concrete contribution to the shear strength.
4. Increasing the steel yield strength or increasing the steel plate thickness of specimens generally increases their shear strength due to the increase in the steel contribution to the shear strength (Nishiyama et al., 2004, Fukumoto and Morita, 2005).
5. Specimens failing in shear, particularly panel-zone shear specimens, exhibit reasonable ductility and deformation capability (Wu et al., 2005, Nishiyama et al., 2004).
6. The load bearing width does not affect the shear strength or the load-displacement behavior of subassembly panel-zone specimens (Koester, 2000).
7. The effects of reducing the D/t ratio were inconclusive. For small-scale specimens, with all other parameters held constant, lower D/t ratios resulted in increased concrete contribution to the shear strength, owing to better confinement. However, this beneficial effect was not observed in full-scale specimen tests with lower D/t ratios (Koester .2000).

Database for Shear Strength

The compiled experimental database was reviewed carefully to identify and include specimens that failed in shear and were shear critical. The following provides additional discussion and rationale for including or excluding specific specimens in the final database for shear strength of rectangular CFST.

- Tomii and Sakino (1979) and Sakino and Ishibashi (1985) reported that their specimens did not have clear shear failures. The specimens developed diagonal shear cracks in the concrete, but both the flanges yielded (due to flexure) at the ultimate state. These specimens were eventually considered flexure critical (with high shear demands), but not shear critical. They were not included in the final database of tests considered for evaluating the shear strength of rectangular CFST.
- Koester (2000) included some specimens that were tested for examining mechanics-based models for shear strength. These specimens had cutouts in the steel webs or different filling material than concrete. These exploratory specimens were not included in the final database.
- For the subassembly specimens tested by Koester (2000), Ricles et al. (2004), Nishiyama et al. (2004), Fukumoto and Morita (2005), and Wu et al. (2005),

the specimens that failed due to weld fracture in the connection, or due to the formation of plastic hinges in the steel beams before shear failure in the panel zones, were not included in the final database. All the specimens that failed in panel-zone shear yielding and failure were included in the final database.

- The specimens tested by Shawkat et al. (2008) could not be included because they were found to be flexure critical. Some of the specimens tested by Ye et al. (2016) could not be included because they had premature weld fracture failure before reaching shear strength.

Simplified Shear Strength Equation for Rectangular CFST

A simplified Equation 17 is proposed to calculate the nominal shear strength, V_n, of rectangular CFST, while accounting for contributions of the steel and concrete. The steel contribution, V_s, is calculated using Equation 18 as the shear strength of the webs of the rectangular cross section, $0.6A_wF_y$. In this equation, A_w is the area of the webs calculated as the total depth, D, minus 2 times half the flange thickness, t_f, multiplied by their thickness, t_w. The concrete contribution, V_c, is calculated using Equation 19 as $0.0316\beta A_c\sqrt{f_c'}$, where f_c' is in ksi and A_c is the area of the concrete infill calculated as the product of the internal dimensions of the cross section, $A_c = bd$. The factor β accounts for the effects of the diagonal compression strut that forms between the load points as shown in Figure 8 when the shear span-to-depth ratio is small. β is calculated using Equation 20a and the shear span-to-depth ratio, a/D. When $a/D \le 0.75$, β is equal to 20. When $a/D > 0.75$, β is equal to 2, which is the typical value for concrete contribution in members.

$$V_n = V_s + V_c \tag{17}$$

where

$$V_c = 0.0316\beta A_c\sqrt{f_c'} \tag{18}$$

$$V_s = 0.6A_wF_y \tag{19}$$

$$\beta = 20 \text{ for } a/D \le 0.75 \tag{20a}$$

$$\beta = 2 \text{ for } a/D > 0.75 \tag{20b}$$

It is important to note that this simplified shear strength equation does not explicitly account for the effect of axial force, P/P_0. It considers the fact that axial compression increases shear strength, and therefore the shear strength calculated for P/P_0 equal to zero (using Equations 17 to 20) will be conservative for situations with higher axial compression. The proposed method accounts for the effects of concrete strut formation through an empirical factor β. It does not account directly or explicitly for the mechanics of compression strut formation in the concrete.

Comparison of Experimental Results with Shear Strength Equations

Because the simplified shear strength equation does not account for the effects of axial force, the final experimental database was parsed into specimens subjected to low levels of axial force ($P/P_0 \le 0.25$), shown in Table 5, and higher levels of axial force ($P/P_0 > 0.25$), shown in Table 6. These tables include the reference source of the specimens and various material and geometric parameters, including the shear span-to-depth ratio, a/D, tube slenderness, D/t, and ratio and axial load, P/P_0. The tables also include the experimental values of shear strength, V_{exp}, and the corresponding flexural moment strength, M_{exp}, in the specimens. The shear strength, V_n, calculated using Equations 17 to 20, and the plastic moment capacity, M_p, calculated according to AISC *Specification* Section I1.2a (2016b), using the plastic stress distribution method while accounting for the effects of axial force, P, are included in the tables. The comparisons of the experimental values of shear strength and corresponding flexural moment with the calculated capacities—that is, V_{exp}/V_n and M_{exp}/M_p—are also included in the tables, and lead to the following statistics. The comparisons of V_{exp}/V_n in Table 5 have a mean value of $\mu = 1.19$, a standard deviation of $\sigma = 0.15$, and a coefficient of variation (CoV) of 0.13. The comparisons of V_{exp}/V_n in Table 6 have $\mu = 1.61$, $\sigma = 0.11$, and a CoV of 0.07. When considered all together, irrespective of the axial load level, the comparisons of V_{exp}/V_n have a $\mu = 1.3$, $\sigma = 0.24$, and a CoV of 0.18. Thus, the proposed simplified shear strength equation is reasonably accurate for specimens with axial load level P/P_0 less than 25%. As expected, the proposed equation is more conservative for specimens with an axial load level P/P_0 greater than 25%. For specimens with $P/P_0 < 0.25$, Figure 13(a) shows the variation of V_{exp}/V_n with respect to the a/D ratio, and Figure 13(b) shows the variation of V_{exp}/V_n with respect to the D/t ratio. For the range of parameters considered, there is no correlation with respect to the a/D ratio or the D/t ratio for these specimens. For the complete database from Tables 5 and 6, including all ratios P/P_0, Figure 14(a) shows the variation of V_{exp}/V_n with respect to the a/D ratio, and Figure 14(b) shows the variation of V_{exp}/V_n with respect to the axial load level P/P_0. As seen in these figures, even for the complete database, there is no correlation with respect to the a/D ratio of the specimens, but increasing the axial load level P/P_0 increases the V_{exp}/V_n ratio and the conservatism of the simplified shear strength equation.

RELIABILITY ANALYSIS

Reliability analyses were conducted to establish an appropriate β factor that should be used in the empirically magnified concrete strength equation to make it possible to use

Table 5. Existing Experiments—Properties, Results, and Comparison with the Proposed Equation for Tests with $P/P_0 < 25\%$																
Specimen	b (in.)	D (in.)	a (in.)	$\frac{a}{D}$	t (in.)	$\frac{D}{t}$	f'_c (ksi)	F_y (ksi)	$\frac{P}{P_0}$	P (kips)	V_{exp} (kips)	V_n (kips)	$\frac{V_{exp}}{V_n}$	M_{exp} (kip-ft.)	M_p (kip-ft.)	$\frac{M_{exp}}{M_p}$
Koester (2000)																
8.4A	8	8	6	0.75	0.25	32	6.2	54.1	0	0	233	214	1.09	116	115	1.01
8.6A	8	8	6	0.75	0.25	32	6.2	54.1	0	0	241	214	1.12	120	115	1.05
8.8A	8	8	6	0.75	0.25	32	6.2	54.1	0	0	237	214	1.11	118	115	1.03
8.4B	8	8	6	0.75	0.375	21	6.0	52.6	0	0	313	262	1.20	156	157	1.00
8.6B	8	8	6	0.75	0.375	21	6.1	52.6	0	0	313	263	1.19	156	157	1.00
8.8B	8	8	6	0.75	0.375	21	5.9	52.6	0	0	316	261	1.21	158	157	1.01
8.B-C	8	8	6	0.75	0.25	32	5.9	61.5	0	0	232	229	1.01	116	129	0.90
8.P-C	8	8	6	0.75	0.25	32	3.9	61.5	0	0	203	213	0.95	101	126	0.81
8.P2-C	8	8	6	0.75	0.25	32	5.9	61.5	0	0	227	229	0.99	113	126	0.90
CFT.2	12	12	9	0.75	0.45	27	7.2	53.1	0	0	571	540	1.06	428	450	0.95
CFT.3	12	12	9	0.75	0.45	27	7.3	53.1	0	0	598	542	1.10	448	450	1.00
CFT.4	12	12	9	0.75	0.45	27	7.4	53.1	0	0	610	543	1.12	457	450	1.02
Nishiyama et al. (2004)																
R1	9.8	9.8	4.9	0.5	0.18	54	16.0	71.3	0.20	383	566	371.3	1.52	228	255	0.90
R2	9.8	9.8	4.9	0.5	0.18	55	7.9	71.3	0.20	240	438	308.9	1.42	177	208	0.85
R3	9.9	9.9	4.9	0.5	0.19	53	14.9	109.6	0.20	425	632	458.1	1.38	255	350	0.73
R4	9.3	9.3	4.9	0.5	0.18	52	14.9	64.1	0.20	328	476	323.6	1.47	192	209	0.92
Fukumoto and Morita (2005)																
SP1	7.9	7.9	5.9	0.75	0.24	33	9.3	74.1	0	0	337	252.7	1.34	179	184	0.97
SP2	7.9	7.9	5.9	0.75	0.35	22	9.3	74.8	0	0	428	316.1	1.35	227	243	0.94
SP3	7.9	7.9	5.9	0.75	0.31	25	17.0	117.2	0	0	554	437.5	1.27	294	373	0.79
Wu et al. (2005)																
FSB-6	15.7	15.7	9.8	0.6	0.24	67	3.7	62.5	0.19	336	602	557.3	1.08	549	562	0.98
FSB-8	15.7	15.7	9.8	0.6	0.31	50	4.2	55.4	0.16	336	659	620.9	1.06	602	636	0.95
FSB-10	15.7	15.7	9.8	0.6	0.39	40	3.9	51.7	0.16	336	669	656.1	1.02	610	707	0.86
Ye et al. (2016)																
S1-1a	4.7	4.7	0.7	0.15	0.08	60	4.6	49.1	0	0	55	49.9	1.10	4.6	12	0.38
S1-1b	4.7	4.7	0.7	0.15	0.08	60	4.6	49.1	0	0	57	49.9	1.14	4.8	12	0.40
S1-2a	4.7	4.7	0.7	0.15	0.08	60	4.6	49.1	0.22	36	65	49.9	1.31	5.5	14	0.39
S1-2b	4.7	4.7	0.7	0.15	0.08	60	4.6	49.1	0.22	36	61	49.9	1.23	5.1	14	0.37

Table 6. Existing Experiments—Properties, Results, and Comparison with the Proposed Equation for Tests with $P/P_0 > 25\%$																
Specimen	b (in.)	D (in.)	a (in.)	$\frac{a}{D}$	t (in.)	$\frac{D}{t}$	f'_c (ksi)	F_y (ksi)	$\frac{P}{P_0}$	P (kips)	V_{exp} (kips)	V_n (kips)	$\frac{V_{exp}}{V_n}$	M_{exp} (kip-ft.)	M_p (kip-ft.)	$\frac{M_{exp}}{M_p}$
Ye et al. (2016)																
S1-3a	4.7	4.7	0.7	0.15	0.08	60	4.6	49.1	0.52	87	82	50	1.64	6.8	10.8	0.63
S1-3b	4.7	4.7	0.7	0.15	0.08	60	4.6	49.1	0.52	87	77	50	1.54	6.4	10.8	0.59
S1-4a	4.7	4.7	0.7	0.15	0.08	60	4.6	49.1	0.65	109	85	50	1.71	7.1	7.1	1.01
S1-4b	4.7	4.7	0.7	0.15	0.08	60	4.6	49.1	0.65	109	85	50	1.71	7.1	7.1	1.00
S2-2a	4.7	4.7	0.7	0.15	0.08	60	4.6	49.1	0.43	73	71	50	1.42	5.9	12.4	0.48
S2-2b	4.7	4.7	0.7	0.15	0.08	60	4.6	49.1	0.43	73	73	50	1.45	6.1	12.4	0.49
S3-1a	4.7	4.7	0.7	0.15	0.08	60	8.3	49.1	0.3	73	100	60	1.68	8.4	17.3	0.48
S3-1b	4.7	4.7	0.7	0.15	0.08	60	8.3	49.1	0.3	73	103	60	1.72	8.6	17.3	0.50
S4-1a	4.7	4.7	0.7	0.15	0.12	40	4.6	60.3	0.32	73	111	67	1.66	9.3	21	0.44

the common-strength reduction factor, ϕ, of 0.9 typically used in the 2016 AISC *Specification*. Reliability analysis is usually conducted to calculate ϕ for values obtained using a proposed strength equation, but calibrating the strength instead is acceptable here given the empirical nature of the magnification for the concrete strength contribution to the total strength. These reliability analyses were conducted using ASCE/SEI 7, Equation C2.3 2 (2016), namely:

$$\phi = \left(\frac{\mu_R}{R_n}\right) e^{-\alpha_R \beta V_R} = PMF e^{-\alpha_R \beta V_R} \tag{21}$$

where β is the reliability index in this case (and not the empirical magnification factor expressed by the same Greek letter). As experiments have shown the shear failure mode of CFST to be ductile, a reliability index of 3.0 was selected. As recommended by ASCE/SEI 7 (2016), the linearization approximation constant, α, was set equal to 0.70 to separate the resistance and demand uncertainties.

In Equation 21, $\left(\frac{\mu_R}{R_n}\right)$ is the mean ratio of the experimental-to-nominal strength calculated using the associated design equation, equal to the product *PMF*, where *P* is the bias (mean ratio) of experimental strength to the strength calculated using measured material properties (i.e., steel coupon and concrete cylinder strengths), *M* is the bias in the material properties calculated as the mean ratio of the measured-to-nominal material strength, and *F* is the bias due to fabrication issues calculated as the mean ratio of the measured-to-nominal cross-sectional properties.

In Equation 21, V_r is calculated as:

$$V_R = \sqrt{V_P^2 + V_M^2 + V_F^2} \tag{22}$$

where

V_F = the coefficient of variation due to fabrication effects

V_M = the coefficient of variation due to material effects

V_P = the coefficient of variation reflecting uncertainties in the design

Circular Concrete-Filled Steel Tubes

For circular CFST, *P* is the mean ratio of the shear strengths V_{exp}/V_n, equal to 1.11 as reported in Figure 5 when using an empirical magnification factor of 18, and with corresponding standard deviation of 0.14 and coefficient of variation, V_p, of 0.13. *M* was assumed to be 1.1 and 1.3 in two contemplated scenarios to bracket the possible expected strength by using R_y values typically reported for steel and concrete individually in the AISC *Seismic Provisions* (2016a). *F* was conservatively taken as 1.0, as recommended by Ellingwood et al. (1980). V_F was taken as 0.05 based on Ravindra and Galambos (1978). For the case where values for steel were used, V_M was taken as 0.07 based on the material property study conducted by Liu (2003). For the case where values for concrete were used, V_M was taken as 0.18 based on MacGregor (1976).

The resulting V_R values obtained considering steel and concrete variability as two independent cases are 0.16 and 0.23, respectively. These resulted in strength reduction factors, ϕ, of 0.88 and 0.90, respectively. These are approximately equal to the strength reduction factor of 0.90 used throughout most of the 2016 AISC *Specification*. Note that the same calibration exercise using an empirical magnification factor of 20 resulted in a strength reduction factor closer to 0.85 and thus, deemed too low to justify using in light of the desirable target of 0.90.

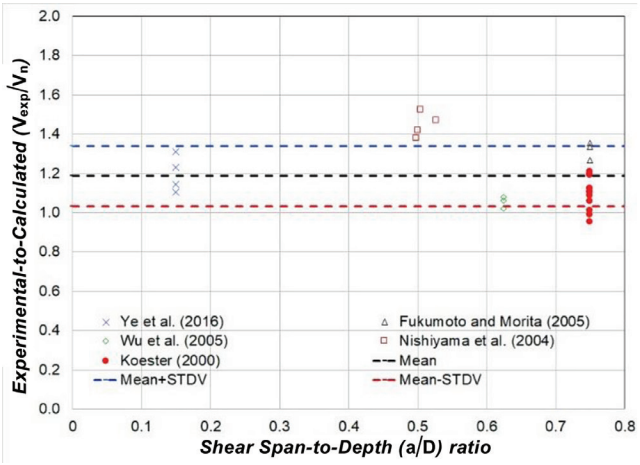

(a) Shear span-to-depth a/D *ratio*

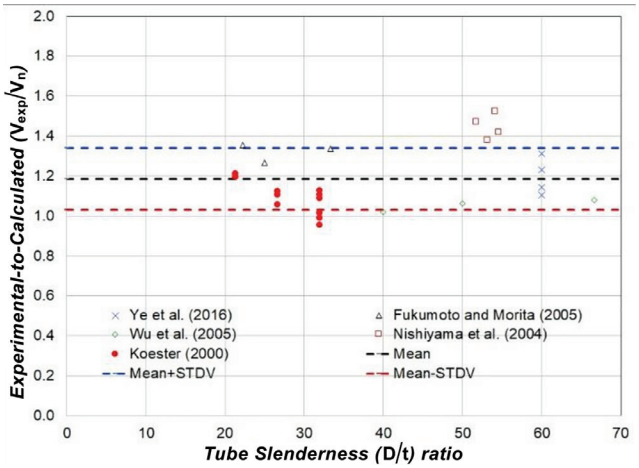

(b) Tube slenderness D/t *ratio*

Fig. 13. Variation of V_{exp}/V_n *for specimens with* $P/P_0 < 25\%$ *from Table 5.*

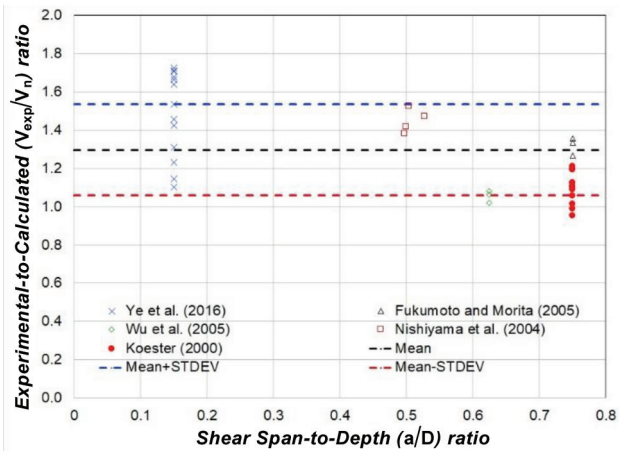

(a) Shear span-to-depth a/D *ratio*

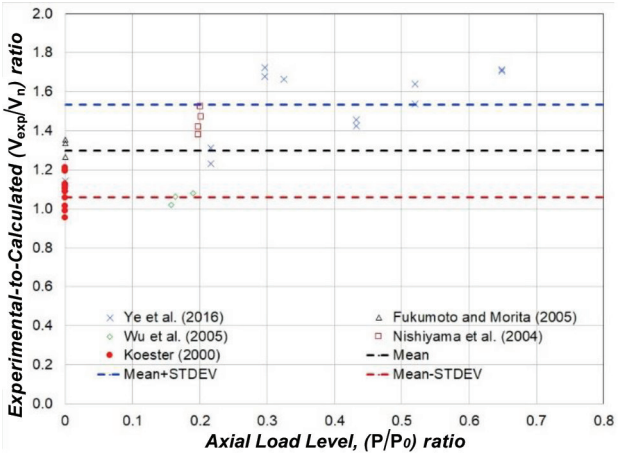

(b) Axial P/P_0 *levels*

Fig. 14. Variation of V_{exp}/V_n *for all specimens included in Tables 5 and 6.*

Rectangular Concrete-Filled Steel Tubes

For rectangular CFST, the reliability analysis was limited to the specimens listed in Table 5 with a low axial load level ($P/P_0 \leq 0.25$). As mentioned earlier, the mean value, μ, of V_{exp}/V_n is 1.19; the standard deviation, σ, is 0.15; and the coefficient of variation, V_P, is 0.13. Similar to circular CFST, $M = 1.3$, $V_M = 0.18$, $F = 1.0$, and $V_F = 0.05$ were considered. The resulting value of ϕ calculated using Equation 21 was equal to 0.96. If the values of M and V_M are changed to 1.1 and 0.07 to be conservative, then the resulting value of ϕ calculated using Equation 21 is equal to 0.94.

PROPOSED INTEGRATED DESIGN EQUATION

On the basis of the results obtained, it is possible to formulate the following integrated requirements for the shear strength of both circular and rectangular CFST, in a format that can directly be introduced into design specifications:

The design shear strength, $\phi_v V_n$, is determined using $\phi_v = 0.90$ and Equation 24 to calculate the nominal shear strength, V_n, as follows:

$$V_n = 0.6A_vF_y + 0.03\beta A_c\sqrt{f_c'} \quad (23)$$

where

A_c = area of concrete in the filled composite member, in.^{2}

A_s = cross-sectional area of steel section, in.^{2}

A_v = shear area of steel, in.^{2}; the shear area for a circular section is equal to $\frac{2A_s}{\pi}$ and, for a rectangular section, is equal to the sum of the area of webs in the direction of in-plane shear

f_c' = concrete strength, ksi

β = 2 for members with $M_u/V_u d \geq 0.7$, where M_u and V_u are equal to the maximum moment and shear demands, respectively, along the member length, and d is equal to the member depth in the direction of bending

β = 20 for members with rectangular cross sections and $M_u/V_u d \leq 0.5$

β = 18 for members with circular cross sections and $M_u/V_u d \leq 0.5$

Linear interpolation between the limiting β values should be used for members with $M_u/V_u d$ between 0.5 and 0.7.

The proposed variation in the value of β reflects the fact that there is a lack of data on the shear strength of circular members for span ratios greater than 0.5. A transition from the β values of 18 and 20 down to the value of 2 is expected, but the exact point at which this happens is unknown, other than the fact that it should occur at a shear span greater than 0.5. Although the experimental data for rectangular members presented in this paper suggests a β value of 20 is acceptable for shear span-to-depth ratios up to 0.75, at this time, a relatively rapid transition to a value of 2 at a shear span of 0.7 is proposed, as illustrated in Figure 15, in superposition to "back-calculated" values corresponding to each of the experimental data considered. More abrupt transitions can be problematic when implemented in design software. A smoother transition is possible and will be considered when more data become available.

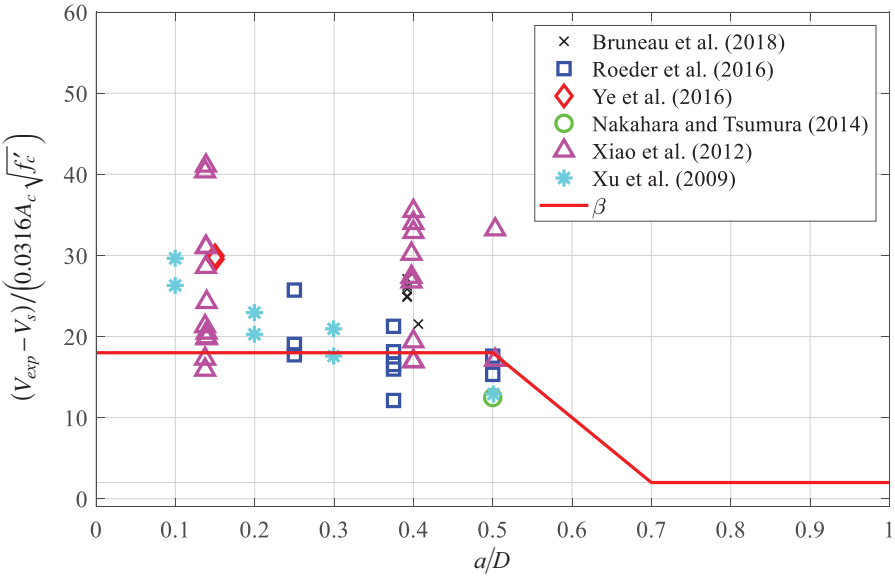

Fig. 15. Recommended transition for β in proposed equations for shear strength of circular CFST.

CONCLUSION

Simplified equations for the shear strength of composite concrete-filled tubes were proposed and calibrated. The format of the proposed equation is consistent for rectangular and circular cross sections, only differing in values used for the shear area and for the β factor resulting from calibration of the ϕ factors. Finite element analysis was performed to compare the expected strength of such composite members with that calculated by the simplified equation. The proposed equation is shown to accurately represent the contribution of the steel tube to the total strength and empirically approximates the contribution of the concrete in composite CFST. Consistent with the philosophy adopted throughout the AISC *Specification* (2016b) and the AISC *Seismic Provisions* (2016a) for various structural members, the contribution of the steel tube is established based on the derived equation for plastic cross-section strength, and this contribution to the total strength of the composite section was confirmed to be accurate by finite element analysis. The contribution of the concrete fill was derived to achieve simple modifications to existing equations, recognizing that a diagonal concrete compression strut provides a significant contribution to that shear strength, but without encumbering the design equations with the complex mathematical expressions that would be required to represent that phenomenon with physical models. The proposed shear strength formula is valid up to a specified shear span-to-diameter ratio.

The effectiveness of the proposed equation was compared with shear test data from the existing literature and was found to be safe. When used with a resistance factor of 0.90, the average ratio of experimental values to calculated values was 1.23 for circular concrete-filled members (1.5 including the experiments with axial loads), with a standard deviation of 0.16 (0.4 including cases with axial load). For rectangular members, the average ratio of experimental values to calculated values was 1.19 for the specimens with axial load level less than 25% (1.61 for the experiments with axial load level greater than 25%) with standard deviations of 0.15 (0.11 for the experiments with axial load level greater than 25%).

Compared to current provisions, the proposed equations utilize the plastic strength of the steel tube and do not cap the strength to the steel tube buckling limit. Also, the proposed equations also reflect that the total strength of the composite section is obtained by summation of steel and concrete strengths and recognize that the concrete strength can be significantly increased by the development of a diagonal compression strut in the concrete, which has been neglected in the current equations.

Future experimental and analytical research is desirable to better understand and quantify the shear strength contribution of the concrete infill for shear spans ratios greater than 0.5, to possibly extend the range of high shear strength to a broader range of applications. Furthermore, given that only a limited number of specimens in past experiments were subjected to a cyclic loading regime, it would be desirable in future research to conduct more inelastic cyclic tests over a more extensive range of parameters to further assess the limits of applicability of the proposed model.

ACKNOWLEDGMENTS

The contributions of the members of the AISC Committee on Specifications Task Committee 5: Composite Members, through discussion and guidance of various ballot proposals, is acknowledged.

REFERENCES

ACI (2011), *Building Code Requirements for Structural Concrete*, ACI 318-11 and commentary, American Concrete Institute, Farmington Hills, Mich.

ACI (2014), *Building Code Requirements for Structural Concrete,* ACI 318-14 and commentary, American Concrete Institute, Farmington Hills, Mich.

AISC (2016a), *Seismic Provisions for Structural Steel Buildings*, ANSI/AISC 341-16, American Institute of Steel Construction, Chicago, Ill.

AISC (2016b), *Specification for Structural Steel Buildings*, ANSI/AISC 360-16, American Institute of Steel Construction, Chicago, Ill.

AIJ (1987), "AIJ Standard for Structural Calculation of Steel Reinforced Concrete Structures," *AIJ 5-26-20*, Shiba, Minato, Tokyo, Japan.

ASCE (2016), *Minimum Design Loads and Associated Criteria for Buildings and Other Structures*, ASCE/SEI 7-16, American Society of Civil Engineers, Reston, Va.

Bruneau, M., Kenarangi, H., and Murphy, T.P. (2018), *NCHRP Research Report 872 Contribution of Steel Casing to Single Shaft Foundation Structural Resistance*, Transportation Research Board, Washington, D.C.

Bruneau, M. and Marson, J. (2004), "Seismic Design of Concrete-Filled Circular Steel Bridge Piers," *Journal of Bridge Engineering*, Vol. 9, No. 1, pp. 24–34.

Ellingwood, B. (1980), *Development of a Probability Based Load Criterion for American National Standard A58: Building Code Requirements for Minimum Design Loads in Buildings and Other Structures*, U.S. Department of Commerce, National Bureau of Standards.

CEN (2005), *Eurocode 3: Design of Steel Structures*, European Committee for Standardization, Brussels, Belgium.

Fischer, E. and Varma, A.H. (2014), "Design of Split-Tee Connections for Special Composite Moment Resisting Frames," *Engineering Journal*, AISC, Vol. 52, No. 3, pp. 185–201.

Fukumoto, T. and Morita, K. (2005), "Elastoplastic Behavior of Panel Zone in Steel Beam-to-Concrete Filled Steel Tube Column Moment Connections," *Journal of Structural Engineering*, Vol. 131, No. 12, pp. 1,841–1,853.

Hajjar, J.F. (2000), "Concrete-Filled Steel Tube Columns under Earthquake Loads," *Progress in Structural Engineering and Materials*, Vol. 2, No. 1, pp. 72–81.

Hajjar, J.F., Gourley, B.C., Tort, C., Denavit, M.D., and Schiller, P.H. (2013), "Steel-Concrete Composite Structural Systems," Department of Civil and Environmental Engineering, Northeastern University, Boston, Mass. http://www.northeastern.edu/compositesystems.

Han, L.H. and Yang, Y.F. (2005), "Cyclic Performance of Concrete-Filled Steel CHS Columns under Flexural Loading," *Journal of Constructional Steel Research*, Vol. 61, No. 4, pp. 423–452.

Kenarangi, H. and Bruneau, M. (2020a), "Investigation of Cyclic Shear Behavior of Circular Reinforced Concrete Filled Steel Tubes," *Journal of Structural Engineering*, 146, No. 5.

Kenarangi, H. and Bruneau, M. (2020b), "Shear Strength of Composite Circular Reinforced Concrete-Filled Steel Tubes," *Journal of Structural Engineering*, Vol. 146, No. 1.

Koester, B. (2000), "Panel Zone Behavior of Moment Connections between Rectangular Concrete-Filled Steel Tubes and Wide Flange Beams," PhD dissertation, Department of Civil and Environmental Engeering, University of Texas-Austin, Austin, Texas.

Lai, Z., Huang, Z., and Varma, A.H. (2017), "Seismic Analysis and Performance of High Strength Composite Special Moment Frames (C-SMFs)," *Structures*, Vol. 9, pp. 165–178.

Lai, Z., Varma, A.H., and Zhang, K. (2014), "Noncompact and Slender Rectangular CFT Members: Experimental Database, Analysis, and Design," *Journal of Constructional Steel Research*, Vol. 101, pp. 455–468.

Leon, R.T., Kim, D.K., and Hajjar, J.F. (2007), "Limit State Response of Composite Columns and Beam-Columns Part I: Formulation of Design Provisions for the 2005 AISC Specification," *Engineering Journal*, AISC, Vol. 44, No. 1, pp. 341–358.

Liu, J. (2003), "Examination of Expected Yield and Tensile Strength Ratios, Report + Addendum Report to AISC," Purdue University, West Lafayette, Ind.

MacGregor, J.G. (1976), "Safety and Limit States Design for Reinforced Concrete," *Canadian Journal of Civil Engineering*, Vol. 3, No. 4, pp. 484–513.

Nakahara, H. and Tsumura, R. (2014), "Experimental Study on Shearing Behavior of Circular CFT Short Column," *Journal of Structural and Construction Engineering (Transactions of AIJ)*, Vol. 79, No. 703, pp. 1,385–1,393.

Nishiyama, I., Fujimoto, T., Fukumoto, T., and Yoshioka, K. (2004), "Inelastic Force-Deformation Response of Joint Shear Panels in Beam-Column Moment Connections to Concrete-Filled Tubes," *Journal of Structural Engineering*, Vol. 130, No. 2, pp. 244–252.

Qian, J., Cui, Y., and Fang, X. (2007), "Shear Strength Tests of Concrete Filled Steel Tube Columns," *Tumu Gongcheng Xuebao (China Civil Engineering Journal)*, Vol. 40, No. 5, pp. 1–9.

Ravindra, M.K. and Galambos, T.V. (1978), "Load and Resistance Factor Design for Steel," *Journal of the Structural Division*, Vol. 104, No. 9, pp. 1,337–1,353.

Ricles, J.M., Peng, S.W., and Lu, L.W. (2004), "Seismic Behavior of Composite Concrete Filled Steel Tube Column-Wide Flange Beam Moment Connections," *Journal of Structural Engineering*, Vol. 130, No. 2, pp. 223–232.

Roeder, C., Lehman, D., and Bishop, E. (2010), "Strength and Stiffness of Circular Concrete-Filled Tubes," *Journal of Structural Engineering*, Vol. 136, No. 12, pp. 1,545–1,553.

Roeder, C., Lehman, D., and Maki, A. (2016), "Shear Design Expessions for Concrete Filled Steel Tube and Reinforced Concrete Filled Tube Components," Washington State Department of Transportation (WSDOT).

Sakino, K. and Ishibashi, H. (1985), "Experimental Studies on Concrete Filled Square Steel Tubular Short Columns Subjected to Cyclic Shearing Force and Constant Axial Force," *Journal of Structural and Construction Engineering (Transactions of AIJ)*, Vol. 353, pp. 81–91.

Shawkat, W., Fahmy, W., and Fam, A. (2008), "Cracking Patterns and Strength of CFT Beams under Different Moment Gradients," *Composite Structures*, Vol. 84, No. 2, pp. 159–166.

Tomii, M. and Sakino, K. (1979), "Experimental Studies on Concrete Filled Square Steel Tubular Beam-Columns Subjected to Monotonic Shearing Force and Constant Axial Force," *Transactions of the Architectural Institute of Japan*, Vol. 281, pp. 81–92.

Varma, A.H., Ricles, J.M., Sause, R., and Lu, L.W. (2002), "Experimental Behavior of High Strength Square Concrete Filled Steel Tube (CFT) Columns," *Journal of Structural Engineering*, Vol. 128, No. 3, pp. 309–318.

Wu, L.Y., Chung, L.L., Tsai, S.F., Shen, T.J., and Huang, G.L. (2005), "Seismic Behavior of Bolted Beam-to-Column Connections for Concrete Filled Steel Tube," *Journal of Constructional Steel Research*, Vol. 61, No. 10, pp. 1,387–1,410.

Xiao, C., Cai, S., Chen, T., and Xu, C. (2012), "Experimental Study on Shear Capacity of Circular Concrete Filled Steel Tubes," *Steel and Composite Structures*, Vol. 13, No. 5, pp. 437–449.

Xu, C., Haixiao, L., and Chengkui, H. (2009), "Experimental Study on Shear Resistance of Self-Stressing Concrete Filled Circular Steel Tubes," *Journal of Constructional Steel Research*, Vol. 65, No. 4, pp. 801–807.

Ye, Y., Han, L.H., Tao, Z., and Guo, S.L. (2016), "Experimental Behaviour of Concrete-Filled Steel Tubular Members under Lateral Shear Loads," *Journal of Constructional Steel Research*, Vol. 122, pp. 226–237.

APPENDIX

Other Shear Strength Equations for Rectangular CFST

Other researchers have also developed and proposed equations for calculating the shear strength of rectangular CFST. These include Koester (2000), AIJ (1987), and Fukumoto and Morita (2005). The equations proposed by Koester were quite similar to the proposed simplified equations, with a few deviations. According to Koester, and as shown in Equation 24, the nominal shear strength, V_{nK}, is the sum of the steel and concrete contributions. The steel contribution is calculated as the shear yield strength of the flat portions of the hollows structural section (HSS) steel tubes used for the specimen. In Equation 25, d_{fl} is the depth of the flat portion of steel tube. The concrete contribution is calculated as $0.0316\beta_K A_c\sqrt{f_c'}$, where β_K is equal to 28 and is slightly larger than the value in Equation 19.

$$V_{nK} = V_{sK} + V_{cK} \tag{24}$$

$$V_{sK} = 0.6F_y(2d_{fl}t_w) \tag{25}$$

$$V_{cK} = 0.0316\beta_K A_c\sqrt{f_c'} \tag{26}$$

$$V_{nF} = V_{sF} + V_{cF} \tag{27}$$

$$V_{sF} = A_w\sqrt{\frac{F_y^2 - f_P^2}{3}} \tag{28}$$

$$V_{cF} = \left(\frac{D_c}{2}\tan\theta + 4\sqrt{\frac{M_{pf}}{D_c f_c'}}\sin\theta\right)D_c f_c' \tag{29}$$

Fukumoto and Morita (2005) proposed Equations 27 to 29 to calculate the panel-zone shear strength of rectangular CFST, particularly those made from higher-strength materials. In Equation 27, V_{nF} is the nominal shear strength, which is the sum of the shear yield strength of the steel tube, V_{sF}, and the shear strength contribution of the concrete infill, V_{cF}. As shown in Equation 28, V_{sF} accounts for the effects of axial compression on the shear yield strength of the steel, where f_P is the axial stress in the steel tube due to the applied compression. As shown in Equation 29, V_{cF} includes the contribution of the main concrete compressive strut and the confining struts resulting from the formation of plastic hinges in the flange plates of the steel tube. In Equation 29, D_c is the depth of the concrete panel, θ is the angle of the concrete strut with respect to the vertical and depends on the a/D ratio, and M_{pf} is the plastic moment capacity of the steel tube flange plate. It is important to note that V_{cF} does not account for the effects of axial compression.

AIJ (1987) provides Equation 31 to calculate the panel-zone shear strength, V_{nJ}, of rectangular CFST:

$$V_{nJ} = \frac{1.2\left(2f_{sc}\gamma v_c + f_{ss}v_s\right)}{d} \tag{31}$$

where

f_{sc} = short-term shear strength of concrete, MPa
= min $(0.05f_c', 0.74 + 0.015f_c')$
γ = $2.5 \times D/d \leq 4.0$ for a square section
d = center-to-center distance between beam flanges, mm
v_c = volume of concrete in the panel, mm^3
f_{ss} = short-term shear strength of steel, MPa
= $F_y/\sqrt{3}$
v_s = volume of steel web of the shear panel, mm^3

It is important to note that V_{nJ} does not account for the effects of axial compression.

These equations were used to calculate the shear strengths of the specimens included in the final database. Table 7 shows the ratios of the experimental-to-calculated shear strength for all the specimens included in Table 5, which had a low axial load level ($P/P_0 \leq 0.25$). As shown by the ratios and the statistical evaluation (μ, σ, and CoV) at the bottom of the table, the Fukumoto and Morita (2005) approach seems to be the most accurate (on average) and with the least CoV. However, it calculates shear strength ratios in the range of 0.80–0.89 for a few specimens tested by Ye et al. (2016). The AIJ (1987) method is the most conservative and has just a couple of ratios less than 1.0. The Koester (2000) approach is also quite accurate (on average), but it does have a few values in the 0.90–0.95 range for specimens tested by Wu et al. (2005) and Ye et al. (2016). The proposed simplified approach is reasonably accurate and has just a couple of ratios less than 1.0.

Table 8 shows the ratios of the experimental-to-calculated shear strength for all the specimens included in Table 6, which had a higher axial load level ($P/P_0 \geq 0.25$).

Table 7. V_{exp}/V_n Ratios for Specimens with $P/P_0 < 0.25$ from Table 5						
Specimen	V_{exp} (kips)	V_n (kips)	$\frac{V_{exp}}{V_n}$	$\frac{V_{exp}}{V_{nK}}$	$\frac{V_{exp}}{V_{nJ}}$	$\frac{V_{exp}}{V_{nF}}$
Koester (2000)						
8.4A	233	214	1.09	1.02	1.22	1.12
8.6A	241	214	1.12	1.05	1.27	1.15
8.8A	237	214	1.11	1.03	1.25	1.13
8.4B	313	262	1.20	1.25	1.25	1.16
8.6B	313	263	1.19	1.25	1.25	1.16
8.8B	316	261	1.21	1.27	1.27	1.18
8.B-C	232	229	1.01	0.96	1.11	1.03
8.P-C	203	213	0.95	0.93	1.00	1.01
8.P2-C	227	229	0.99	0.94	1.09	1.01
CFT.2	571	540	1.06	1.02	1.16	1.01
CFT.3	598	542	1.10	1.07	1.22	1.06
CFT.4	610	543	1.12	1.08	1.24	1.07
Nishiyama et al. (2004)						
R1	566	371	1.52	1.27	1.56	1.08
R2	438	309	1.42	1.22	1.46	1.23
R3	632	458	1.38	1.21	1.36	1.01
R4	476	324	1.47	1.22	1.56	1.08
Fukumoto and Morita (2005)						
SP1	337	253	1.34	1.19	1.41	1.15
SP2	428	316	1.35	1.33	1.31	1.14
SP3	554	438	1.27	1.21	1.20	0.96
Wu et al. (2005)						
FSB-6	602	557	1.08	0.93	1.19	1.24
FSB-8	659	621	1.06	0.93	1.16	1.14
FSB-10	669	656	1.02	0.93	1.08	1.07
Ye et al. (2016)						
S1-1a	55	50	1.10	0.90	0.91	0.80
S1-1b	57	50	1.14	0.94	0.95	0.83
S1-2a	65	50	1.31	1.07	1.09	0.95
S1-2b	61	50	1.23	1.01	1.02	0.89
		Average	1.19	1.09	1.21	1.06
		Standard deviation	0.15	0.14	0.17	0.11
		CoV	0.13	0.13	0.14	0.11

Table 8. V_{exp}/V_n Ratios for Specimens with $P/P_0 > 0.25$ from Table 6						
Specimen	V_{exp} **(kips)**	V_n **(kips)**	$\frac{V_{exp}}{V_n}$	$\frac{V_{exp}}{V_{nK}}$	$\frac{V_{exp}}{V_{nJ}}$	$\frac{V_{exp}}{V_{nF}}$
Ye et al. (2016)						
S1-3a	82	50	1.64	1.34	1.36	1.22
S1-3b	77	50	1.54	1.26	1.27	1.14
S1-4a	85	50	1.71	1.40	1.42	1.29
S1-4b	85	50	1.71	1.40	1.41	1.29
S2-2a	71	50	1.42	1.17	1.18	1.05
S2-2b	73	50	1.45	1.19	1.21	1.07
S3-1a	100	60	1.68	1.34	1.40	0.99
S3-1b	103	60	1.72	1.38	1.44	1.02
S4-1a	111	67	1.66	1.45	1.39	1.21
		Average	1.62	1.33	1.34	1.14
		Standard deviation	0.11	0.10	0.10	0.12
		CoV	0.07	0.07	0.07	0.10

As shown by the ratios and the statistical evaluation (μ, σ, and CoV) at the bottom of the table, the Fukumoto and Morita (2005) approach seems to be the most accurate (on average), but this is incidental because the approach did not actually account for the effects of axial compression on concrete shear strength contribution. This can be explained further as follows. For the Ye et al. (2016) specimens, the shear span-to-depth ratio is extremely small (0.075), which leads to very high concrete contributions (V_{cF}). This causes overestimation of shear strengths for low axial load cases in (shear strength ratios in the 0.80–0.95 range) and seemingly appropriate prediction for high axial load cases in Table 8 (shear strength ratios in the 0.99–1.29 range). Both the AIJ (1987) and the Koester (2000) approaches are also conservative with respect to the test results. The proposed simplified approach is the most conservative for higher axial load levels.